

CRWR Online Report 14-01

Inundation Modeling of a Potential Glacial Lake Outburst Flood in Huaraz, Peru

By

Marcelo A. Somos-Valenzuela

Rachel E. Chisolm

Daene C. McKinney

Denny Rivas

March 2014

CENTER FOR RESEARCH IN WATER RESOURCES

Bureau of Engineering Research • The University of Texas at Austin

J.J. Pickle Research Campus • Austin, TX 78712-4497

This document is available online via World Wide Web at

<http://www.crwr.utexas.edu/online.shtml>

High Mountains Adaptation Partnership

Inundation Modeling of a Potential Glacial Lake Outburst Flood in Huaraz, Peru

This report was produced for review by the United States Agency for International Development (USAID). It was prepared by The University of Texas at Austin and The Mountain Institute for Engility under Contract EPP-I-00-04-00024-00 order no 11

IQC Contract No. AID-EPP-I-00-04-00024

Task Order No. AID-OAA-TO-11-00040

March 2014

DISCLAIMER

The author's views expressed in this publication do not necessarily reflect the views of the United States Agency for International Development or the United States Government

Inundation Modeling of a Potential Glacial Lake Outburst Flood in Huaraz, Peru

Marcelo Somos-Valenzuela, Rachel Chisolm, Daene McKinney, Denny Rivas

Center for Research in Water Resources

University of Texas at Austin, Austin, Texas USA

ABSTRACT

One of the consequences of recent glacier recession is the formation and rapid growth of lakes formed at the snout of glaciers. One risk is that moraines damming these glacial lakes could fail releasing a huge volume of water and creating a glacial lake outburst flood. This happened December 13, 1941, at Lake Palcacocha, Peru, flooding the city of Huaraz and killed several thousand people. Recently Lake Palcacocha has been declared in a state of emergency state because its volume has again reached dangerous levels, threatening a flood that would quickly reach Huaraz causing major devastation and potentially loss of life. An analysis has been performed of the glacial hazards for the city of Huaraz from Lake Palcacocha. This analysis consists of physical models of each process in the chain of events that results in a glacial lake outburst flood: rock and ice avalanche; wave generation, propagation and moraine overtopping; terminal moraine breaching and draining of the lake; and downstream inundation and impacts in the city of Huaraz. Two scenarios of moraine erosion were simulated: a worst-case event of a 56 m breach and a smaller 22.5 m erosion event. These scenarios showed that flood reaches the City of Huaraz 1.06 and 1.20 hours after the avalanche for the 56 m and 22.5 m events, respectively. The inundation in the city is extensive in both breaching events with depths exceeding 1 m in many areas, especially near the channel of the Quillcay River, and the velocity of the flood exceeding 1 m/s in most of this area. Because of the inundation depth and the velocity of the flow, most of the area of the city that experiences flooding will have a very high hazard level, putting both lives and property at risk.

CONTENTS

Section	page
Contents	i
List of Figures	iii
List of Tables	v
1. Introduction	6
2. Study Area	8
3. Methodology	9
3.1. Physical Information	11
3.1.1. Digital Elevation Model	11
3.1.2. Roughness Coefficient Values	11
3.2. Avalanche Simulation	16
3.3. Lake Simulation	17
3.3.1. Empirical Wave Model	17
3.3.2. Lake Simulation	18
3.4. Moraine Breach Simulation	20
3.4.1 Empirical Breach Equations	20
3.4.2 MIKE-11 Moraine Breach Model	21
3.5. Inundation Simulation	27
3.6. Hazard Identification	30
4. Results	31
4.1. Avalanche Simulation	31
4.2. Lake Simulation	32
4.3. Moraine Breach Simulation	36
4.4. Inundation Simulation	38
4.5. Inundation in Huaraz	43

4.6. Hazard Identification	48
5. Conclusions	53
Acknowledgements	54
References	54

LIST OF FIGURES

Figure	page
Figure 1. Lake Palcacocha in 2010 with Palcaraju (6,274m) on the left and Pucaranra (6,156 m) on the right in the background (photo by Colette Simonds)	7
Figure 2. Map of the study area showing Lake Palcacocha and the city of Huaraz in the Quilcay watershed.....	9
Figure 3. Aerial photograph of the Quilcay watershed showing Lake Palcacocha, the Paria River and the City of Huaraz. Source: Horizons (2013)	10
Figure 4. Digital Elevation Model (DEM) of Quillcay watershed.	12
Figure 5. NDVI results using reflection corrected Landsat 7 image values.	15
Figure 6. Land cover classification according to the ISODATA classification.	15
Figure 7. Lake Palcacocha moraine showing the breach of the 1941 GLOF.	24
Figure 8. Partial longitudinal profile of Lake Palcacocha and the terminal moraine.	24
Figure 9. Maximum potential breach: (Top) breach shape, (Bottom) overlapping between the potential breach and existing terrain cross-sections across the last 200 m of eroded moraine.	25
Figure 10. Palcacocha Lake volume/depth curve. Volume is mainly concentrated above 4500 m (60 m depth measured from the surface).....	26
Figure 11. Paria River canyon (Quebrada Cojup) looking downstream.....	29
Figure 12. Wave for the large avalanche scenario represented by fluid depth just after the avalanche enters the lake	33
Figure 13. Wave for the large avalanche scenario at its maximum height: (top) orthographic view and (bottom) wave profile	34
Figure 14. Wave for the large avalanche scenario at the point of overtopping the terminal moraine: (top) orthographic view and (bottom) wave profile	35

Figure 15. Hydrograph of discharge at the lake outlet due to wave overtopping for the large avalanche scenario.....	36
Figure 16. Maximum and minimum potential outflow hydrographs from Lake Palcacocha due to a moraine breach.....	37
Figure 17. Combined wave overtopping and 56m and 22m breaching hydrographs.	38
Figure 18. Cross-sections for FLO-2D Simulation Results.....	40
Figure 19. Hydrographs at cross-sections for the 56 m breach event.....	41
Figure 20. Hydrographs at cross-sections for the 22.5 m breach event.....	41
Figure 21. Flood depth versus time at cross-section 4 for the 56 m and 22.5 m breach events. .	43
Figure 22. Water depth from GLOF inundation in Huaraz from combined hydrograph for 56 m breach event.....	45
Figure 23. Water depth from GLOF inundation in Huaraz from combined hydrograph for 22 m breach event.....	46
Figure 24. Maximum velocity of the flood waters in Huaraz for the large avalanche scenario for 56 m breach event.....	47
Figure 25. Maximum velocity of the flood waters in Huaraz for the large avalanche scenario for 22 m breach event.....	48
Figure 26. Hazard level in Huaraz from Lake Palcacocha GLOF for large avalanche scenario for the 56 m breaching event.....	50
Figure 27. Hazard level in Huaraz from Lake Palcacocha GLOF for large avalanche scenario for the 22 m breaching event.....	51
Figure 28. Time to maximum flood depth for the large avalanche scenario for the 56 m breaching event.	52
Figure 29. Time to maximum flood depth for the large avalanche scenario for the 22 m breaching event.	53

LIST OF TABLES

Table	page
Table 1. Roughness Coefficient Values for the Paria River (FLO-2D, 2012).....	14
Table 2. Moraine Breach Parameters for the 56 m and 22.5 m Breaches.....	26
Table 3. Debris Flow Event Hazard Level.....	31
Table 4. Characteristics of RAMMS Simulated Avalanches for Three Scenarios.	31
Table 5. Waves Calculated for Three Avalanche Scenarios Using Empirical Method.	32
Table 6. Waves Calculated for Large Avalanche Scenario Using Flow-3D Model.	33
Table 7. Location of Flood Hydrograph Cross-sections Downstream of Lake Palcacocha	39
Table 8. Flo-2D Simulation Results at Cross-sections Downstream of Lake Palcacocha.....	42

1. INTRODUCTION

Continued atmospheric warming has induced melting of many glaciers around the world (WGMS 2012, IPCC 2013). The formation of new lakes in de-glaciating high-mountain regions strongly influences landscape characteristics and represents a significant hazard related to climate change (Frey *et al.* 2010; Rosenzweig *et al.* 2007; Kattleman 2003; Richardson and Reynolds 2000). The glacier-covered area in the Cordillera Blanca range of Peru has decreased from a Little Ice Age peak of 900 km² to about 700 km² in 1970, 528 km² in 2003, and further to 482 km² in 2010 (UGRH 2010; Burns and Nolin 2014). As a consequence of this glacier recession, many lakes have formed or expanded in the Cordillera Blanca that pose various levels of Glacial Lake Outburst Flood (GLOF) risk for communities below these lakes (Emmer and Vilímek 2013). In particular, Lake Palcacocha situated above the city of Huaraz caused a devastating GLOF in 1941 and has grown to dangerous levels in recent years.

Steep summits in the Cordillera Blanca are undergoing long-term slope destabilization due to warming and degrading permafrost. Related ice and rock avalanches are especially dangerous in connection with lakes forming at the foot of the steep mountain walls because they can trigger large waves in the lakes and potentially lead to GLOFs (Carey *et al.* 2012; Haeberli 2013). There are many examples in the Cordillera Blanca of historical to recent glacier-related incidents and catastrophes (Carey 2010; Portocarerro 2014). A recent example is the 2010 ice/rock avalanche from the summit of Nevado Hualcán that fell into Lake 513 and generated waves that overtopped the dam of the lake producing flood waves and debris flows reaching the town of Carhuaz (Carey *et al.* 2012; Schneider *et al.* 2014). Preventive lowering of Lake 513 by artificial tunnels in the 1990s created a freeboard of 20 meters and helped avoid a major catastrophe where many people could have been killed (Carey *et al.* 2012; Portocarerro 2013).

Trigger effects leading to avalanches include earthquakes, snowmelt, heat waves, and heavy precipitation (Haeberli 2013; Huggel *et al.* 2010). Emmer and Vilímek (2013, 2014) and Haeberli *et al.* (2010) recommend that the evaluation of hazards posed by glacial lakes be based on systematic and scientific analysis of lake types, moraine dam characteristics, outburst mechanisms, down-valley processes and possible cascades of processes. In addition, changes in climate patterns are likely to increase the frequency of avalanches as a consequence of reduced stability of permafrost, bedrock and steep glaciers in the Cordillera Blanca (Fischer *et al.* 2012).



Figure 1. Lake Palcacocha in 2010 with Palcaraju (6,274m) on the left and Pucaranra (6,156 m) on the right in the background (photo by Colette Simonds)

Lake Palcacocha (Figure 1) poses an increasing glacial lake hazard in the Cordillera Blanca. In 1941 a GLOF occurred from the lake that flooded the city of Huaraz, killing more than 5000 people (according to best estimates) and destroying infrastructure and agricultural land all the way to the coast (Carey 2010). In recent years, Lake Palcacocha has grown to the point where it is once again dangerous. Avalanches from the steep surrounding slopes can now reach the lake directly, creating the potential for generating waves that could overtop the moraine dam and reach the city of Huaraz (Hegglin and Huggel 2008). In 2010 the lake was declared to be in a state of emergency because its level exceeded the height deemed safe (Diario la Republica 2010). Siphons have been installed at the lake recently to temporarily lower the water surface about three meters, but lowering it 15 m or more is recommended for safety now and in the

future (Portocarrero 2014). The lake's damming moraine could possibly fail if an avalanche generated wave overtops the moraine and abruptly releases a large volume of water from the lake creating a flood wave and/or debris flow (Instituto Nacional de Defensa Civil 2011). Local authorities and people living in Huaraz are concerned about the threat posed by Lake Palcacocha, and they have requested technical support to investigate the impacts that a GLOF could have on Huaraz and methods to reduce the risk.

This paper describes an analysis of the processes involved, the behavior and consequences of a potential GLOF from Lake Palcacocha, and the resulting inundation in Huaraz. The process cascade starts from an avalanche falling into the lake resulting in a wave that overtops the moraine causing a breach and ensuing downstream flooding and inundation in the City of Huaraz. In the following sections the setting of the problem is presented followed by a description of available data used to model the processes. Then the physical basis and modeling of each of the processes in the chain are described, followed by results of each of these and concluding with details of the inundation at Huaraz resulting from a large avalanche event.

2. STUDY AREA

Lake Palcacocha (Figure 1) is located at 9°23' S, 77°22' W at an elevation of 4,562 m in the Ancash Region of Peru and is part of the Quillcay watershed in the Cordillera Blanca (Figures 2 and 3). The lake has a maximum depth of 73 m and an average water surface elevation of 4562 m. The outlet of the lake flows into the Paria River, a tributary of the Quillcay River that passes through the City of Huaraz to the Santa River, the main river of the region. Prior to the 1941 GLOF, the lake had an estimated volume of 10 to 12 million m³ of water (Instituto Nacional de Defensa Civil 2011). After the 1941 GLOF, the volume was reduced to about 500,000 m³. In 1974, drainage structures were built at the lake to maintain 8 m of freeboard at the lake outlet, a level thought to be safe from additional avalanche generated waves. Due to the growth of the lake in the up-glacier direction, the lake volume increased to about 17 million m³ of water by 2009, exceeding the level that is safe (Instituto Nacional de Defensa Civil 2011). The siphon system has been able to reduce the level of the lake by 3-5 m providing a total free board of about 12 m.

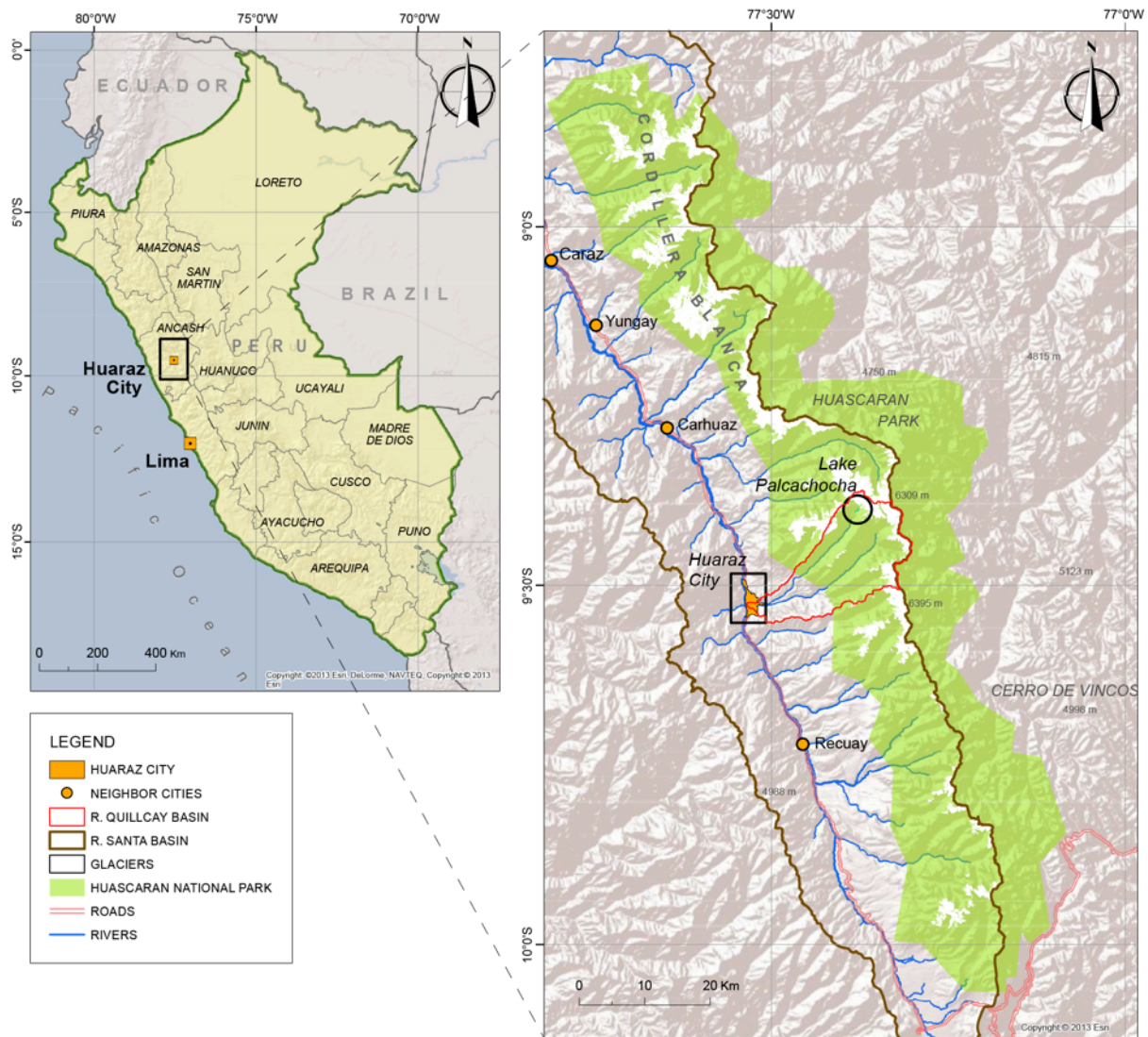


Figure 2. Map of the study area showing Lake Palcacocha and the city of Huaraz in the Quillcay watershed.

3. METHODOLOGY

We consider a chain of events that could result in an avalanche triggered GLOF from Lake Palcacocha and assess the potential inundation of Huaraz from such an event. The assumed trigger for the GLOF is an avalanche from the Palcaraju or Pucaranra glaciers located directly above the lake. Three different avalanche sizes are considered: small (0.5 million m³), medium (1 million m³) and large (3 million m³). When the avalanche enters the lake the resulting wave

can overtop the damming moraine, which has 8-12 m of freeboard, and initiate an erosive breaching process that could release considerable amounts of water to the Paria River and potentially inundate densely populated areas of Huaraz. The process chain from avalanche to inundation was simulated using several models: potential avalanches were modeled using RAMMS (Christen *et al.* 2010), lake wave dynamics were modeled with FLOW-3D (Flow Science 2012), hydrographs of the potential GLOF discharge from the moraine breach were generated using MIKE-11 (DHI 2001), and propagation of the flood wave downstream and inundation in Huaraz were calculated using FLO-2D (O'Brien 2003).

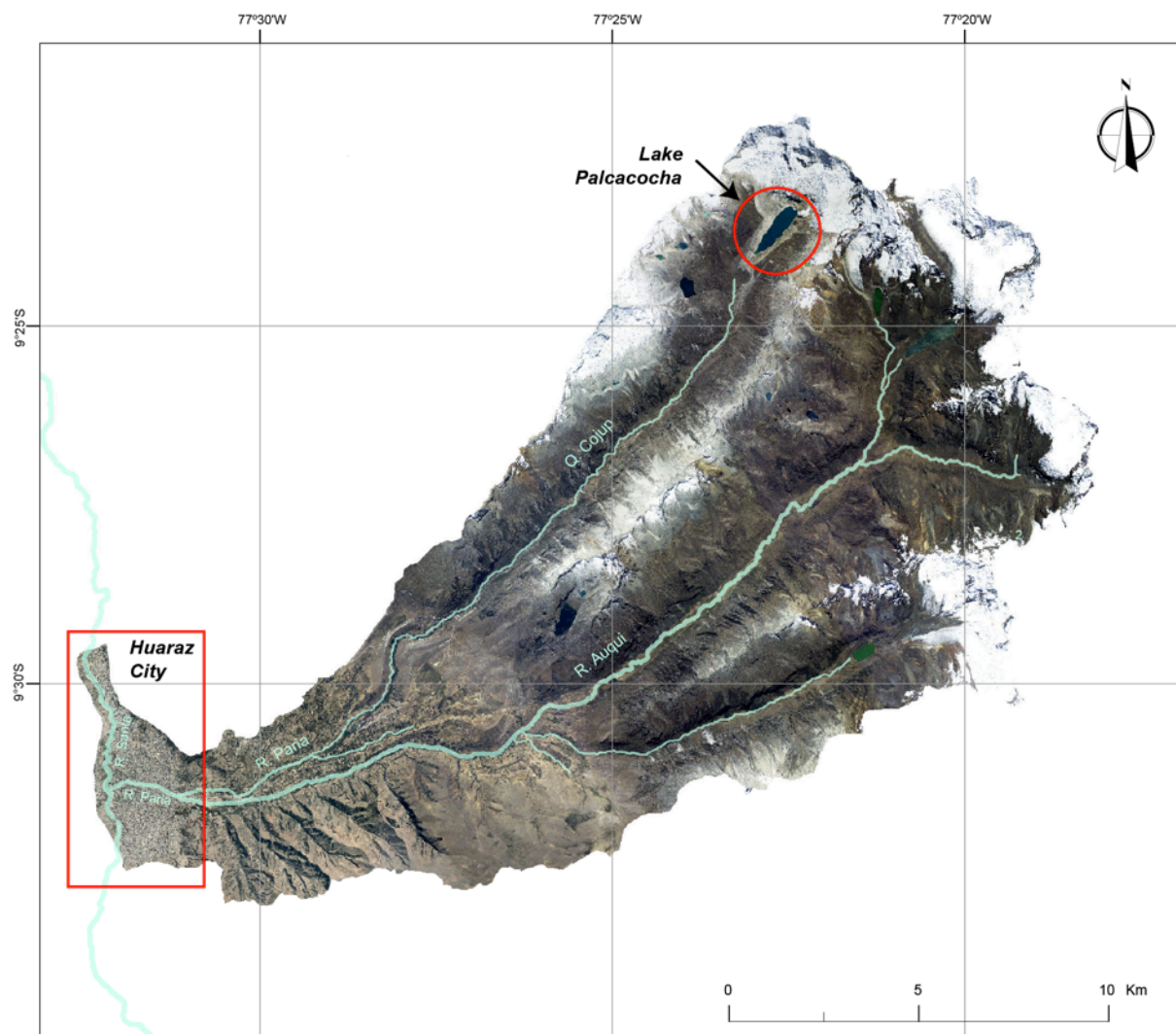


Figure 3. Aerial photograph of the Quilcay watershed showing Lake Palcacocha, the Paria River and the City of Huaraz. Source: Horizons (2013)

3.1. Physical Information

3.1.1. DIGITAL ELEVATION MODEL

A 5m \times 5m horizontal resolution digital elevation model (DEM) generated exclusively for this work was used (Horizons 2013) (Figure 4) using high-resolution Laser Imaging, Detection and Ranging (LIDAR) techniques, which provide vertical accuracies of up to 7 cm. A set of ten Ground Control Points (GCP), temporarily established to support the LIDAR flights, allowed control, calibration and adjustment of the LIDAR data, and orthorectification of high-resolution aerial images. A drainage line dataset created by the Geographic-Military Institute of Perú was used to verify the DEM information and provide the streamline of the Paria River, which drains from Lake Palcacocha as well the Quillcay, and Rio Santa streamlines.

The Unidad de Glaciología y Recursos Hídricos of Peru's National Water Authority (UGRH) carried out a bathymetric survey of Lake Palcacocha in 2009 that was used to represent the elevation of the lake bottom in the DEM (UGRH 2009). The distance from the moraine damming Lake Palcacocha to the Rio Santa is 22 km. However, besides the urban center of the City of Huaraz, other isolated infrastructures are spread between the lake and the city, including small houses, a primary school, fish farms, and water supply facilities.

3.1.2. ROUGHNESS COEFFICIENT VALUES

Flow resistance in river channels depends on different factors such as: meandering, bed channel materials, cross-sectional area and its variation, obstructions, and vegetation (Chow, 1959). For the inundation model, values of Manning's roughness coefficient need to be estimated and included as input to the simulation (Flow Science 2012). Estimates of roughness coefficients can be done *in situ*. However, this is time consuming and can be inefficient for large river reaches; also, the spatial variability of roughness may be misrepresented (Forzieri *et al.* 2011; Hossain *et al.* 2009). As an alternative, automatic classification of vegetation indices (VIs) derived from spectral images can be combined with high resolution terrain elevation maps (Forzieri *et al.*, 2011; Forzieri *et al.* 2010). The VI is used to classify the different land cover classes present in the river basin and the elevation map is used to estimate cover texture, which is used to estimate roughness values. Roughness values can be assigned to different land covers

either manually or automatically (Forzieri *et al.* 2011, 2010). We have used a combination of the two procedures mentioned above and the scheme developed by Hossain *et al.* (2009), which is an adaptation of Hamandawana *et al.* (2006). The procedure calculates the normalized differential vegetation index (NDVI) from a multispectral image; then, an Iterative Self-Organizing Data Analysis Technique (ISODATA) is used to determine the number of classes into which the pixels in an image can be classified (Ball and Hall 1965). Finally, sliding representation is used to assign roughness coefficient values to the classes.

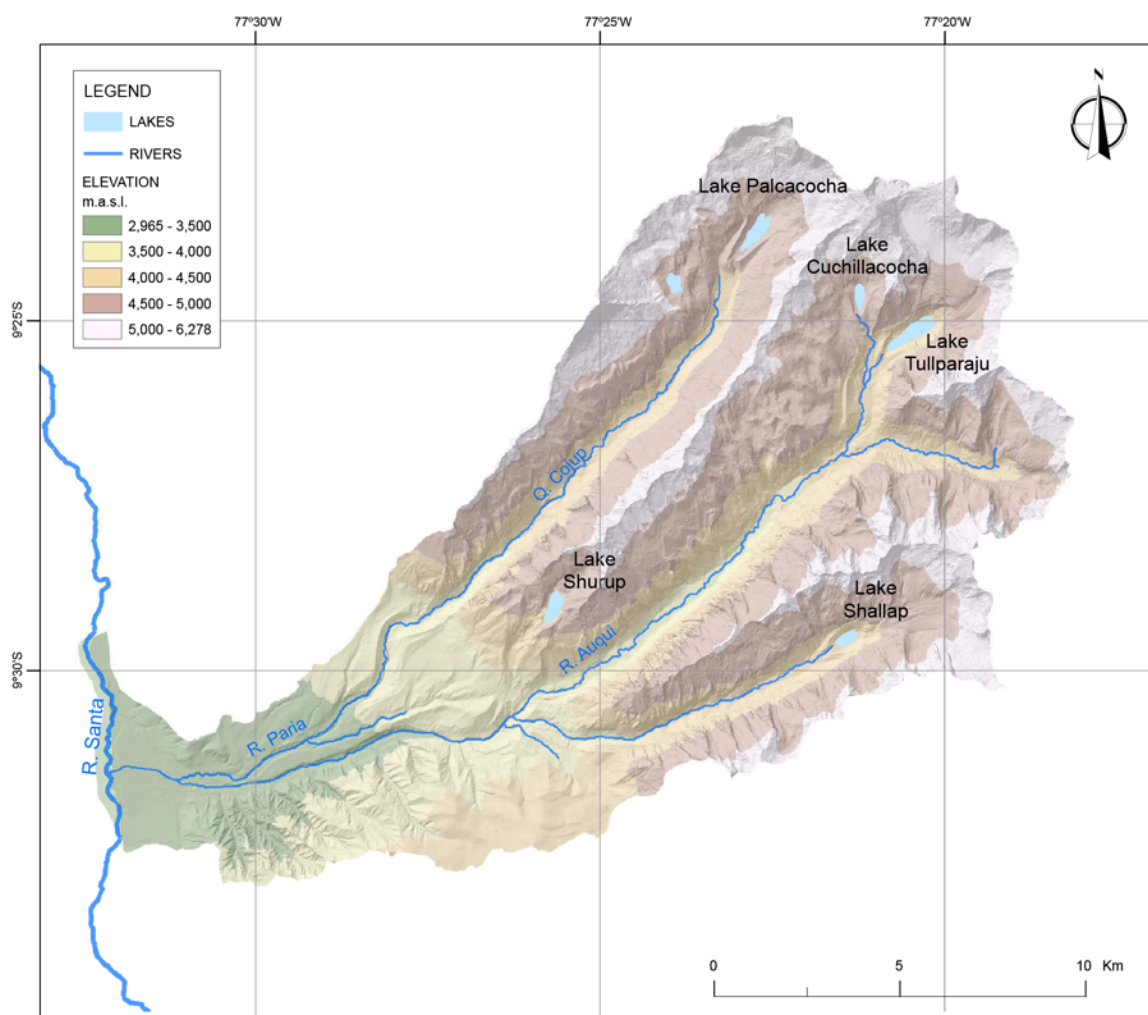


Figure 4. Digital Elevation Model (DEM) of Quillcay watershed.

Landsat 7 Band 3 (near infrared 0.77-0.90 μm) and Band 4 (red 0.63-0.69 μm) from an October 22, 2013 image (WRS_PATH 8, WRS_ROW 67)¹ were used to calculate NDVI values to assess the presence of live green vegetation (Rouse *et al.* 1973).

$$NDVI = \frac{(Band_4 - Band_3)}{(Band_4 + Band_3)} \quad (1)$$

NDVI values range from -1 to 1, and higher values indicate the presence of more live green vegetation. The raw digital number (DN) from the image was adjusted by converting it to irradiance for both bands and then to reflectance (Chander and Markham 2003; Chander *et al.*, 2009). The adjustments produce more consistent NDVI values since they consider sun elevation, acquisition date, and gain/bias settings of the sensors for each band.

The ISODATA scheme (Ball and Hall 1965) minimizes the variability within clusters and categorizes pixels into a number of classes based on minimizing the sum of squared distances between each pixel and its assigned cluster center, equivalent to minimizing the Mean Squared Error (MSE) (Hossain *et al.* 2009)

$$MSE = \frac{\sum_{\forall x} [x - C(x)]^2}{(N - c)b} \quad (2)$$

where $C(x)$ is the mean of the cluster that contains pixel x , N is the number of pixels, c is the number of clusters, and b is the number of spectral bands. Finally, density sliding was implemented based on the threshold values generated using the NDVI raster. ISODATA classification using a modified method of Hossain *et al.* (2009) in which ISODATA classification is applied to the multispectral image.

We inspected the Paria River from Lake Palcacocha to the Rio Santa in June-July 2013, and we have combined our field observations with the automatic classification results. Although there are a considerable number of land cover types, we use 5 main classes that are most representative of the system. In addition, the variation of the roughness coefficient values for the different land cover types present in the area is minimal. Table 1 shows the roughness coefficient values assigned according to the land cover observed in the field.

¹ U.S. Geological Survey–EROS Data Center, <http://landsat.usgs.gov/>

Figure 5 shows the NDVI values taken from the Landsat 7 image after the reflectance correction (Chander *et al.*, 2009). For the higher NDVI values, more intense vegetation is present. Along the main stream of the Paria River (below the lake and above the city) more green vegetation is present, which is corroborated by the field observations. In the area of Huaraz, there are low NDVI values indicating a decrease in green area. The ISODATA classification was performed on the NDVI raster data (Figure 6). Finally, using the ISODATA raster, we assigned the maximum, minimum and maximum roughness coefficient values from Table 1, and the values are used in the FLO-2D inundation calculations described below.

Table 1. Roughness Coefficient Values for the Paria River (FLO-2D, 2012)

#	Class Type	Class Description	Min.	Max
1	Urban	Concrete	0.10	0.15
2	Bare Soil	Earth, Rock, Gravel	0.05	0.013
3	Cultivated Areas or grass	No Crop or short grass	0.06	0.22
4	Tree	Cleared land with tree stumps, no sprouts	0.30	0.40
5	Natural Streams	Mountains Streams, no vegetation in channel, banks usually steep, trees and brush along banks submerged at high stages. Bottom: Cobbles with large boulders	0.04	0.07

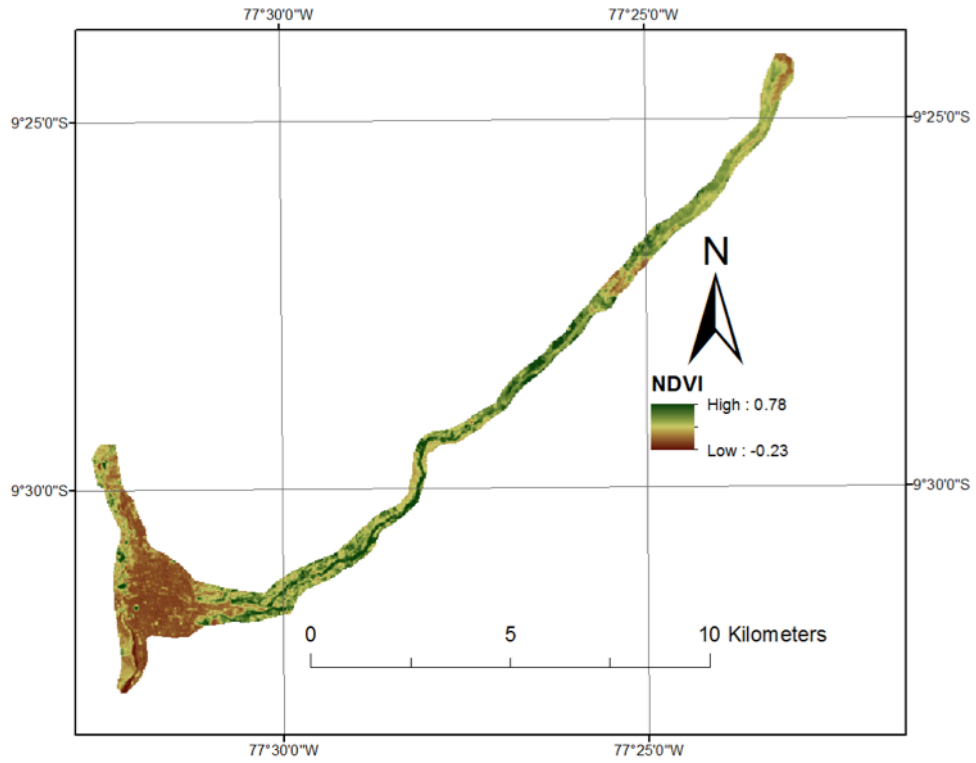


Figure 5. NDVI results using reflection corrected Landsat 7 image values.

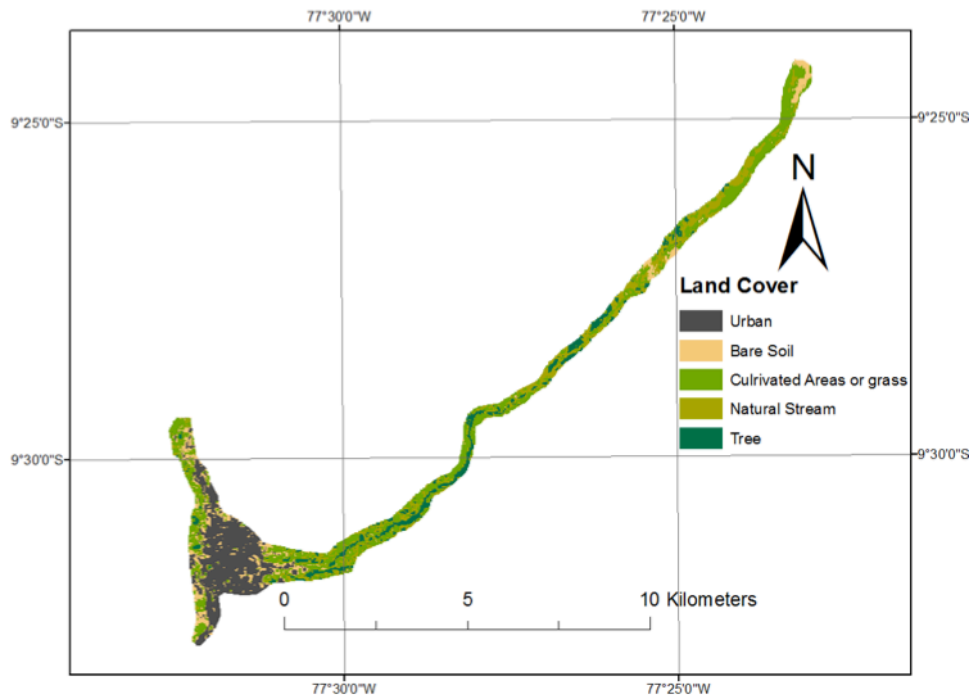


Figure 6. Land cover classification according to the ISODATA classification.

3.2. Avalanche Simulation

In non-forested areas, avalanches can be generated on slopes of 30-50° and even less in tropical areas (Christen *et al.*, 2005; Haeberli 2013). The mountains surrounding Lake Palcacocha have slopes up to 55°; therefore, they have a high chance of generating avalanche events. Nonetheless, it is difficult to forecast when avalanches will occur and where the detachment zone will be located (Evans and Clague, 1988; Haeberli *et al.*, 2010).

In order to predict the behavior of an avalanche into Lake Palcacocha, a recent avalanche that occurred at nearby Lake 513 in 2010 (Carey *et al.* 2012; Schneider *et al.* 2014) is used as a model due to some similar conditions between the two locations. In particular, the lakes are geographically close and oriented in the same east-west direction, the elevation of lakes and surrounding peaks are very similar, the lake depths are similar, and the glaciers in contact with the lakes have similar characteristics. The primary difference is the lake outlet damming condition, which is loose moraine material at Lake Palcacocha, but solid rock at Lake 513.

Three avalanche scenarios are considered with volumes of 0.5 (small), 1.0 (medium), and 3.0 (large) million m³, respectively, similar to those that Schneider *et al.* (2014) used for assessment of Lake 513 based on recommendations of practice for Switzerland (Raetzo *et al.* 2002). The Rapid Mass Movements (RAMMS) avalanche model was used to model the progression of the avalanche down the mountain to Lake 315 (Christen *et al.* 2010). RAMMS solves two-dimensional, depth-averaged mass and momentum equations on three-dimensional terrain using a finite volume method (Bartelt *et al.* 2013). The inputs for the model include: (1) terrain data (a DEM); (2) the avalanche release area; (3) fracture heights; and (4) friction parameters. The model computes the velocity of the avalanche, the distance of the run out, the pressure distribution, and the height of the avalanche front at different locations below the initiation point.

RAMMS is based on a finite-volume solution to the equations of motion for granular flows over general three-dimensional topography (Bartelt *et al.* 2013; Christen *et al.* 2008). The governing equation of mass conservation is (Christen 2010)

$$\frac{\partial h}{\partial t} + \frac{\partial(hV_x)}{\partial x} + \frac{\partial(hV_y)}{\partial y} = \dot{Q} \quad (3)$$

where Q denotes the mass production source term. The governing equations of momentum conservation are (Christen 2010)

$$\frac{\partial hV}{\partial t} + \frac{\partial}{\partial x} \left(hV_x^2 + gk \frac{h^2}{2} \right) + \frac{\partial}{\partial y} (hV_x V_y) = S_{gx} - S_{fx} \quad (4)$$

$$\frac{\partial hV}{\partial t} + \frac{\partial}{\partial x} (hV_x V_y) + \frac{\partial}{\partial y} \left(hV_y^2 + gk \frac{h^2}{2} \right) = S_{gy} - S_{fy} \quad (5)$$

where S_{gx} and S_{gy} are the gravitational forces in the x and y directions, respectively, k is the earth pressure coefficient and S_f is the frictional force. The model uses the Voellmy friction relation to describe the flowing friction

$$S_f = \mu \rho g h \cos(\phi) + \frac{\rho g V^2}{\xi} \quad (6)$$

where S_f is the friction slope, ρ is the density of the rock and ice (kg/m^3), g is the gravitational acceleration (m/s^2), ϕ is the slope, h is the avalanche height (m) normal to the bed and V is the avalanche velocity (m/s). The Coulomb-friction term (the first term on the right hand side) with a dry surface friction (μ) dominates the total friction when the flow is relatively slow and the turbulent friction parameter (second term) (ξ) tends to dominate the total friction when the flow is rapid as in an avalanche such as those considered here (Bartelt *et al.* 2013; Christen *et al.* 2010, 2008). In the RAMMS avalanche model, we use $\xi = 1000 \mu/\text{s}^2$, $\mu = 0.12$ and $\rho = 1000 \text{ kg/m}^3$, values similar to those used to model the avalanche into Lake 513 (Schneider *et al.* 2014).

3.3. Lake Simulation

3.3.1. EMPIRICAL WAVE MODEL

The empirical method of Heller *et al.* (2009) for calculating the characteristics of slide-generated impulse waves has been tested with laboratory studies and field observations. Although this method has its limitations, it can be used for comparison with hydrodynamic model results; if the characteristics of the impulse wave in both the hydrodynamic model and empirical model are of the same order, a reasonable confidence may be placed in the model results.

The Heller *et al.* (2009) method was used to determine the characteristics of the avalanche-generated waves to be used as a baseline comparison for the waves generated in the FLOW-3D simulations; the wave characteristics calculated according to this empirical method are compared with the characteristics of the waves generated in FLOW-3D to ensure that the simulations of the avalanche impact and wave generation are producing reasonable results. The avalanche characteristics (width, thickness and velocity at lake entry) are used as inputs to this empirical model along with the dimensions of the lake and the densities of the slide material and water. The characteristics of the avalanche-generated waves are determined according to the following equations (Heller *et al.* 2009).

The wave height is predicted as

$$H(x) = \frac{3}{4}h \left[P \left(\frac{x}{h} \right)^{-0.33} \right]^{0.8} \quad (7)$$

where P is the impulse product parameter

$$P = FS^{0.5}M^{0.25} \left[\cos \left(\frac{6\alpha}{7} \right) \right]^{0.5} \quad (8)$$

h is the water depth (m), $S = s/h$ is the relative avalanche thickness, s = avalanche thickness (m), and α = avalanche impact angle (degrees), $F = V_s/\sqrt{gh}$ is the avalanche Froude number, V_s = avalanche velocity (m/s), $M = \rho_s \nabla_s / (\rho_w b h^2)$ = relative avalanche mass, ρ_s = avalanche density (kg/m³), ρ_w = water density (kg/m³), and ∇_s = avalanche volume (m³). Because of the irregularity of the lakebed and the shallow water depth in the portion of the lake near the terminal moraine, the empirical method of Heller *et al.* (2009) cannot be used to accurately predict the overtopping depth or volume. The moraine overtopping is simulated in FLOW-3D as described in the following section.

3.3.2. LAKE SIMULATION

The empirical equations provide the height and location of the maximum wave height, but not the dynamics of the wave as it moves across the lake or the hydrograph at the outlet. For this purpose, FLOW-3D, a three-dimensional fluid dynamic modeling software that uses the volume of fluid method for modeling free surface flows (Flow Science 2012) is used to model

the avalanche generated waves, its propagation and the overtopping of the terminal moraine. The primary output from the model is a hydrograph generated for each avalanche scenario that can be used as an input for a downstream GLOF model.

FLOW-3D solves the mass continuity equation and the Navier-Stokes equations for Lake Palcacocha

$$V_F \frac{\partial \rho}{\partial t} + \frac{\partial}{\partial x} (\rho u A_x) + \frac{\partial}{\partial y} (\rho v A_y) + \frac{\partial}{\partial z} (\rho w A_z) = R_{DIF} + R_{SOR} \quad (9)$$

where V_F is the fractional volume open to flow, ρ is the fluid density, R_{DIF} is the turbulent diffusion term, R_{SOR} is the mass source, u, v, w are the velocity components and A_x, A_y, A_z are the fractional areas open to flow in the x, y, z directions, respectively.

$$\frac{\partial u}{\partial t} + \frac{1}{V_F} \left(u A_x \frac{\partial u}{\partial x} + v A_y R \frac{\partial u}{\partial y} + w A_x \frac{\partial u}{\partial z} \right) = -\frac{1}{\rho} \frac{\partial p}{\partial x} + G_x + f_x - \frac{R_{SOR}}{\rho V_F} (u - u_w - \delta u_s) \quad (10)$$

$$\frac{\partial v}{\partial t} + \frac{1}{V_F} \left(u A_x \frac{\partial v}{\partial x} + v A_y R \frac{\partial v}{\partial y} + w A_x \frac{\partial v}{\partial z} \right) = -\frac{1}{\rho} \frac{\partial p}{\partial y} + G_y + f_y - \frac{R_{SOR}}{\rho V_F} (v - v_w - \delta v_s) \quad (11)$$

$$\frac{\partial w}{\partial t} + \frac{1}{V_F} \left(u A_x \frac{\partial w}{\partial x} + v A_y R \frac{\partial w}{\partial y} + w A_x \frac{\partial w}{\partial z} \right) = -\frac{1}{\rho} \frac{\partial p}{\partial z} + G_z + f_z - \frac{R_{SOR}}{\rho V_F} (w - w_w - \delta w_s) \quad (12)$$

where G_i are body accelerations, and f_i are viscous accelerations in the $i = x, y, z$ directions, respectively, u_i, v_i, w_i are source components ($i = w$) and relative source surface ($i = s$) velocities in the x, y, z directions.

For free surface flows in FLOW-3D, the volume of fluid function (F) defined in Equation 13 determines what volumes are occupied by fluid at any given time and point in space. For free surface flows, $F=1$ in the regions occupied by the fluid, and $F=0$ in void regions

$$\frac{\partial F}{\partial t} + \frac{1}{V_F} \left[\frac{\partial}{\partial x} (F u A_x) + R \frac{\partial}{\partial y} (F v A_y) + \frac{\partial}{\partial z} (F w A_z) \right] = F_{DIF} + F_{SOR} \quad (13)$$

where F_{DIF} is the diffusion term and F_{SOR} is the time rate of change of F due to a source. The turbulence model used for these simulations is the k- ϵ RNG (Renormalized Group) model with dynamically computed turbulent mixing lengths based on the flow conditions.

The bathymetry data to be used for the hydrodynamic lake model are taken from a 2009 bathymetric survey done by the UGRH. The data from the bathymetric survey have been extracted to a 5 m grid that has been embedded into the digital elevation model of the

surrounding terrain that is described in Section 3.1. This combined topography of the lakebed and surrounding terrain is used as input to the lake model.

The impact of the avalanche with the lake is modeled as a volume of water equal to the avalanche volume that enters the lake from the terrain above. To reproduce the avalanche characteristics, the average velocity and depth of the volume of water at the point of impact is matched with the velocities and depths of the avalanche as it enters the lake. The height and depth of the initial fluid volume representing the avalanche are adjusted until the depth and velocity of the water just before impact with the lake are approximately the same as the corresponding values in the avalanche model. The key to accurately representing the wave generation in the FLOW-3D model is reproducing the transfer of mass and momentum from the avalanche to the lake. The details of this process are not well understood, and the problem of reproducing an avalanche generated wave in a hydrodynamic model is not an easy one because of the complicated dynamics of mixing and dissipation of energy that occur at the point of impact.

3.4. Moraine Breach Simulation

3.4.1 EMPIRICAL BREACH EQUATIONS

Flood risk in locations downstream of a natural earthen dam depends on the capacity of the dam to hold the impounded water. That capacity threshold can be exceeded due to overtopping wave events or collapse of the dam induced by structural failures or erosive processes. In glacial lakes, both kinds of failure are likely to occur; moraine dams are susceptible to erosive destruction, and they can be overtopped by high waves produced by avalanches.

The erosive phenomenon that drives earthen dam breaks is not fully understood. The complex interaction between soil and fluid dynamics that govern the dam erosion process still presents a research challenge. Different methods have been explored to predict breach development across earthen dams and the resulting outflow hydrographs (Wahl 2004). The first type involves deterministic models that partially describe the governing physics of the problem. The second type is applied extensively in engineering practice to predict the characteristics of a dam breach and maximum peak flows by applying empirical statistical models based on recorded

historical events of dam failures. As long as the obstacles to the development and application of deterministic models remain, empirical models represent a reasonable alternative to assess dam breach problems.

The growth process of the moraine breach in Lake Palcacocha will control the release of water impounded by the moraine in the case of failure. Regardless of the type of trigger that starts the erosion process, the shape and magnitude of the outflow hydrograph are dependent on the expanding rate and shape of the breach. That breaching mechanism is difficult to predict without detailed knowledge of the geotechnical composition of the moraine. Moreover, breach erosion is commonly arrested by processes that are largely unpredictable in numerical models (O'Connor *et al.* 2001).

The physical parameters required to apply the empirical equations include: the volume of impounded water, the water depth from the lake surface to the final level reached by the breach, the volume of moraine material to be eroded, and the moraine width. These parameters can be extracted from digital bathymetry and terrain models, but a potential breach shape must first be defined to determine the potential limits of breach growth. Following Froehlich (1995) the peak discharge, Q_p (m³/s), is given by

$$Q_p = 0.607(V^{0.295}h^{1.24}) \quad (14)$$

and the failure time, t_f (hr) is

$$t_f = 0.00254(V^{0.53}h^{-0.9}) \quad (15)$$

where h (m) is water depth and V (m³) is the water volume.

3.4.2 MIKE-11 MORaine BREACH MODEL

The empirical dam breach equations in the previous section provide the peak discharge and the failure time of the breach, but they do not provide the full hydrograph of discharge for the breach process. The numerical model MIKE-11 is used for this. We have no data of an actual breaching event to compare the results of the simulations with or calibrate the model. Instead, the simulation has two objectives: (1) to reasonably validate the peak flow and failure

time values estimated by the empirical equations, and (2) to produce the hydrographs that those empirical equations are not able to provide.

Because we lack the precise geotechnical and erodability characteristics of the Lake Palcacocha moraine, we follow two main criteria to define the potential shape and depth of the breach. First, we assume that the easiest path for water to flow through will be the path defined by the 1941 GLOF. That breach remains and it seems reasonable that a new flood will flow in the same way as the 1941 flood. Second, though the breach depth may vary somewhat, due to the magnitude and continuity of the trigger mechanism (avalanche generated wave overtopping), the worst-case event is the most appropriate scenario for planning possible mitigating measures (Laenen *et al.* 1987). Likewise, in the absence of bedrock and given the presence of low cohesion materials are unlikely to prevent large-scale breaches from forming in the Lake Palcacocha moraine (C. Portocarrero, 2013, personal communication). There is some uncertainty about the depth to bedrock at the moraine and we have assumed two different levels of possible moraine erosion (56 m and 22.5 m) as discussed below. Figure 8 shows the cross-section through the moraine based on the lake bathymetry and the DEM.

The profile in Figure 8 shows three elevation layers associated with different moraine dimensions and impounded water volumes. The surface of the upper layer (0-22.5 m depth) is immediately exposed to erosion, and it is comprised of materials with less cohesive properties that increase its susceptibility to failure. In order to reach the bottom of the second layer, the breach must go to a depth of 56 m, longitudinally erode over 985 m of moraine material, and be able to drain $16.4 \times 10^6 \text{ m}^3$ of water. There are no estimates of the probability of the latter event, but uncertainty on internal conditions of the moraine structure does not allow us to reject the hypothesis that such an event might actually happen. Therefore, we have considered two potential breaches due to a large avalanche event and associated wave, one that erodes the moraine to a breach depth of 56 m and a smaller one that has a breach depth of 22.5 m. The breach depth of 56 m is the worst-case scenario. If the third layer of the moraine were to be exposed, a relatively small volume of water would remain - $0.8 \times 10^6 \text{ m}^3$ or about 5% of the entire water volume. To release that volume, which we consider very unlikely, over 1700 m of moraine material must be eroded in the longitudinal direction, extending the breach 700 m longer than the length developed in the second layer.

For the 56 and 22.5 m breaches, the depth of the water is not equal to the depth of the breach since the depth of breach includes the freeboard at the top part of the moraine above the invert of the drainage structure. The difference is 6.3 m because the overtopping wave discharge does not include the entire avalanche volume, $0.5 \times 10^6 \text{ m}^3$ of the wave volume is retained in the lake and $2.5 \times 10^6 \text{ m}^3$ is released in the overtopping discharge. Therefore, the residual lake volume increases both the volume (by $0.5 \times 10^6 \text{ m}^3$) and depth of the lake (by 1.7 m) before the erosive process starts. In the overtopping, we assume that the top part of the moraine (8 m above the drainage tunnel invert level) is instantaneously destroyed. The erosion rate is uniformly distributed below that level. The volume of impounded water released in the breaching process increases once the wave passes through the lake. Figure 8 shows static conditions before the chain of processes starts, while Table 2 shows the after-wave condition.

The discharge through the breach in the moraine will progressively enlarge the downstream channel until the breach intersects the bottom of the second layer. Since moraine erosion is a backward moving process (moving from the downstream face to the upstream face of the moraine), we project the potential breach shape as a deeper extension of the last channel segments created by the 1941 GLOF. This shape will propagate backwards to form the whole breach as shown in Figure 9, reshaping the existing terrain cross-sections with the projected maximum potential breach. The projected breach shape for the 56 m breach (Figure 9a) is 50 m wide at the bottom level, with slopes of 1H:1V, and a maximum depth of 54 m. The bottom width of the breach and downstream channel are approximately equal at the lowest elevation of the second layer (Figure 9b).

The Lake Palcacocha volume/elevation curve (Figure 10) was derived from bathymetry measurements (UGRH 2009). The parameters resulting from combining the estimated maximum potential breach shape, lake geometry and surrounding digital terrain model are shown in Table 2. These parameters are the inputs required by the empirical models that estimate the peak outflow and failure time of the moraine breach process. Note that the volume of impounded water accounts for the volume of water susceptible to being drained through the maximum potential breach (water above the bottom of the second layer), including the additional volume added by a potential avalanche minus the overtopping volume from the surge wave generated by the avalanche.



Figure 7. Lake Palcacocha moraine showing the breach of the 1941 GLOF.

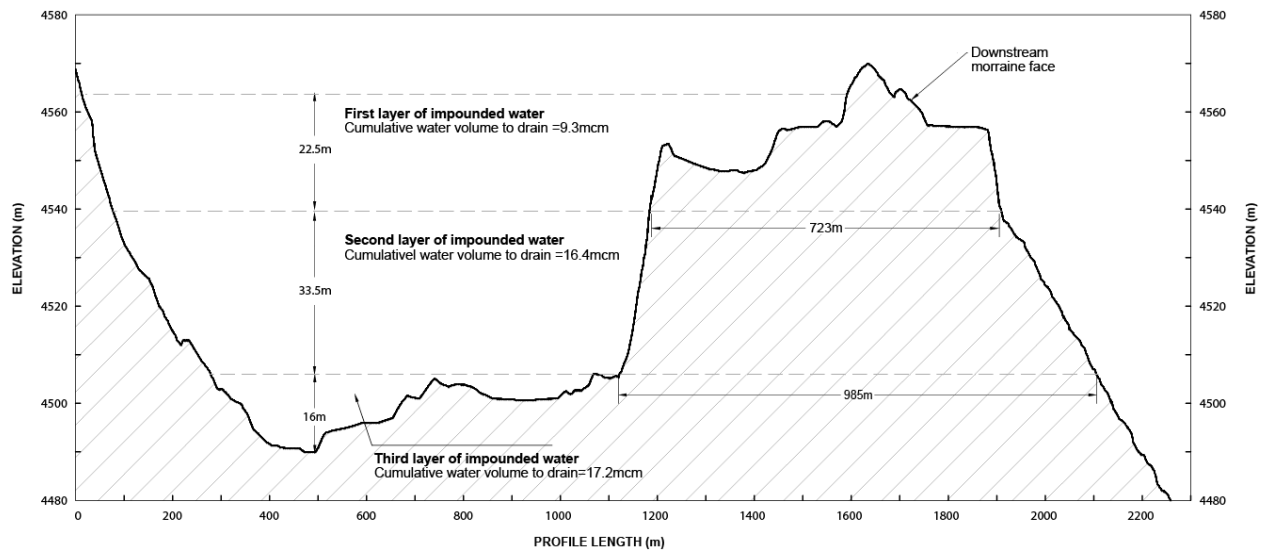


Figure 8. Partial longitudinal profile of Lake Palcacocha and the terminal moraine.

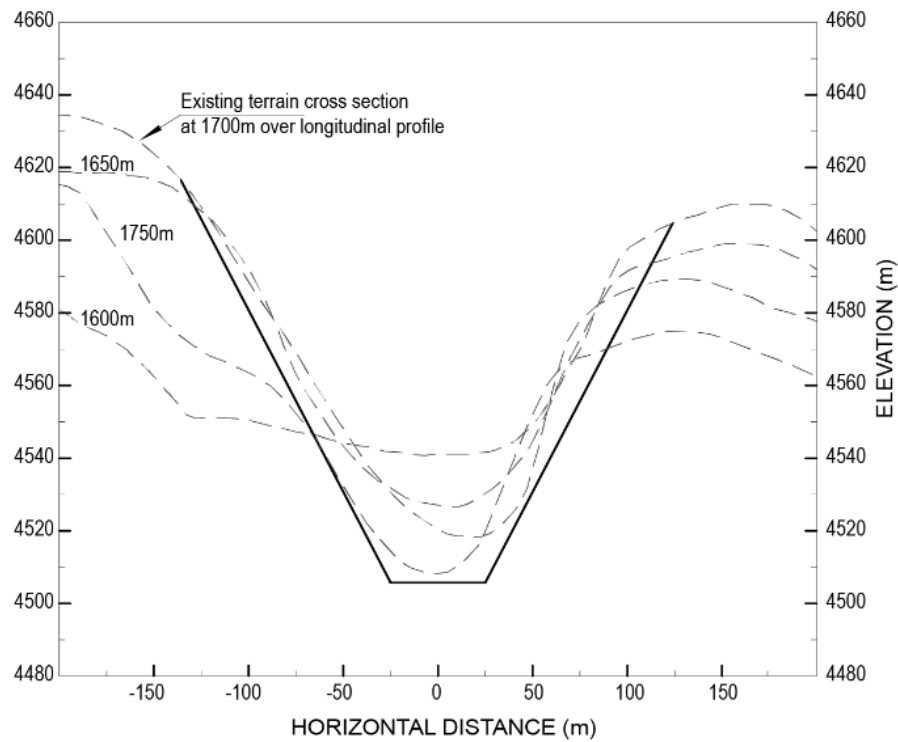
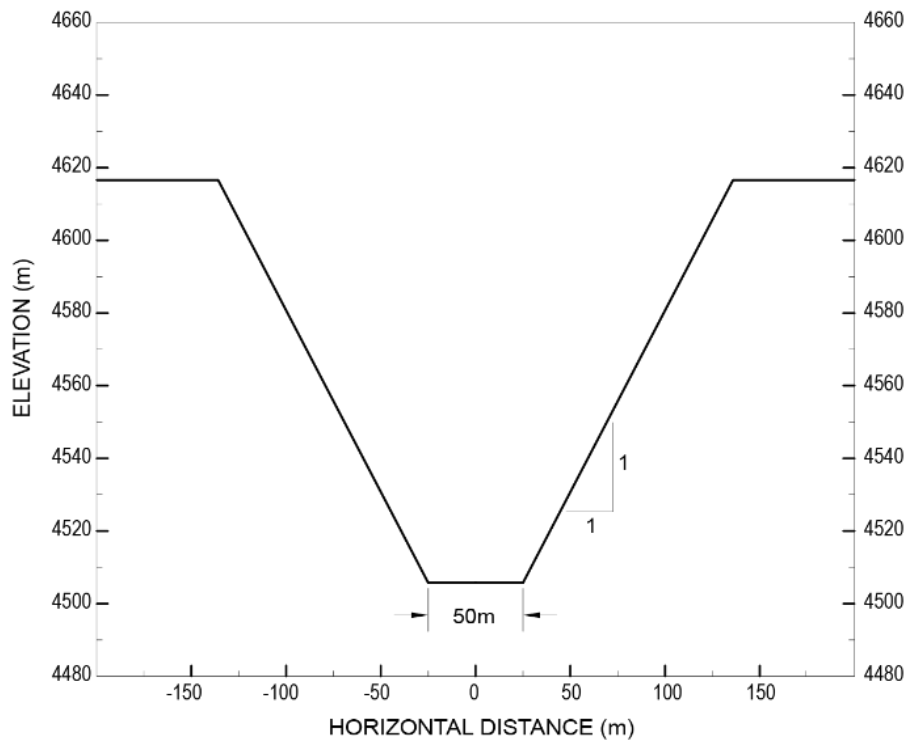


Figure 9. Maximum potential breach: (Top) breach shape, (Bottom) overlapping between the potential breach and existing terrain cross-sections across the last 200 m of eroded moraine.

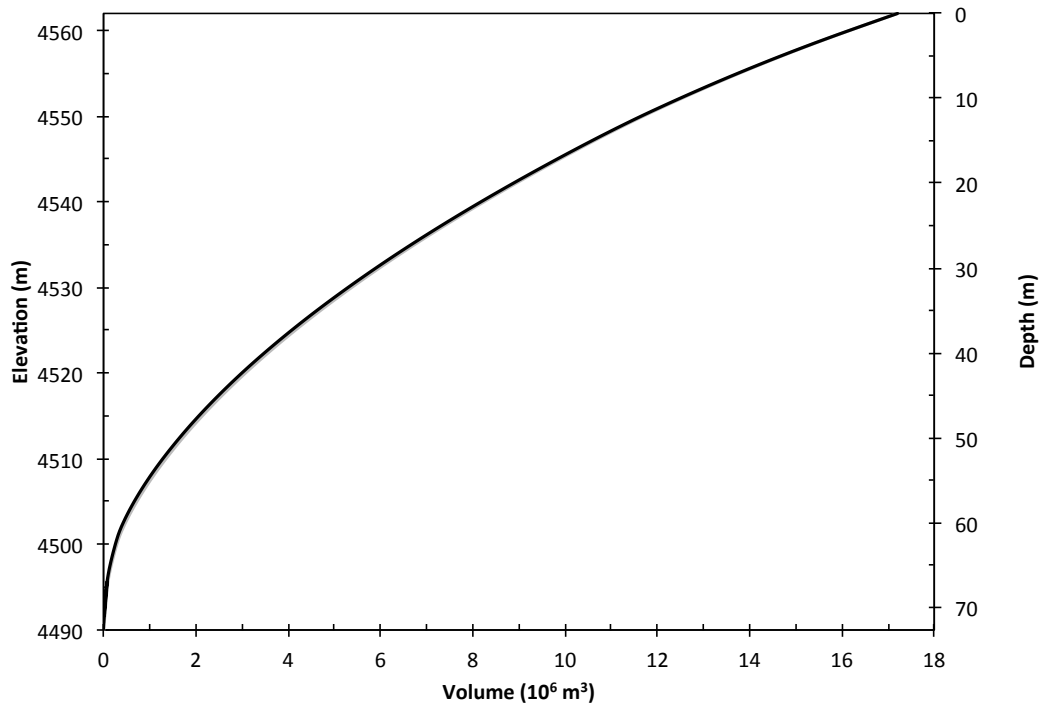


Figure 10. Palcacocha Lake volume/depth curve. Volume is mainly concentrated above 4500 m (60 m depth measured from the surface).

Table 2. Moraine Breach Parameters for the 56 m and 22.5 m Breaches.

Parameter	Value
56 m Breach	
Depth of water (h)	49.7 m
Volume of impounded water not including the lower zone (V)	$16.9 \times 10^6 \text{ m}^3$
Depth of the Breach (h_d)	56.0 m
22.5 m Breach	
Depth of water (h)	16.2 m
Volume of impounded water not including the lower zone (V)	$9.8 \times 10^6 \text{ m}^3$
Depth of the Breach (h_d)	22.5 m

To generate moraine breach hydrographs, numerical simulations of Lake Palcacocha and the moraine were computed using the US National Weather Service (NWS) DAMBRK dam-breach method (Fread 1979) implemented in MIKE-11 software (DHI 2011). The model represents outflow as if the growing moraine breach were a broad crested weir, for which the breach shape changes over time and critical flow exists during the entire breaching period (DHI 2011). The parameters used to set the moraine breach model for Lake Palcacocha in MIKE-11 are: impounded lake geometry, surrounding terrain topography, breach shape and variable failure times; basically the same parameters applied to the empirical equations described in the previous section, including the elevation-volume curve.

Fourteen different empirical dam breach models were compared to the results of a hydraulic simulation using NWS-DMBRK in MIKE-11 (Rivas *et al.* 2014). Those results suggest that for Lake Palcacocha the differences between the empirical and MIKE-11 moraine breach models are smallest when the Froehlich model is used. The peak flow difference is less than 1% and the failure time difference is about 21%. The Froehlich model requires fewer parameters to estimate peak outflow than the rest of the equations that were considered. That simplicity reduces the uncertainty implicitly added by including erodability conditions in models such as those proposed by Xu and Zhang (2009), Peng and Zhang (2011), Walder and O'Connor (1997), or MacDonald and Landridge-Monopolis (1984), for which the failure time differences range approximately between 51% and 99%.

3.5. Inundation Simulation

FLO-2D is used to calculate the flooding downstream of Lake Palcacocha. The model is suitable to simulate the propagation of the debris flow (FLO-2D, 2012). The conservation of mass equation solved in FLO-2D is

$$\frac{\partial h}{\partial t} + \frac{\partial(hv)}{\partial x} = i \quad (16)$$

and the conservation of linear momentum equation is

$$S_f = S_o - \frac{\partial h}{\partial x} - \frac{v}{g} \frac{\partial v}{\partial x} - \frac{1}{g} \frac{\partial v}{\partial t} \quad (17)$$

where h (m) is the flow depth, v (m/s) is the depth-averaged velocity in one of the flow directions, i is the excess rainfall intensity (m/s), S_f is the friction slope, S_o is the bed slope. We are considering the effects of sediments; consequently, the characteristics of sediment and its concentration in the fluid are included. Thus the total friction slope can be expressed as (Flo-2, 2012; Julien 2010; O'Brien *et al.* 1993)

$$S_f = S_y + S_v + S_{td} = \frac{\tau_y}{\gamma_m h} + \frac{K\eta\omega}{8\gamma_m h^2} + \frac{n^2\omega^2}{h^{4/3}} \quad (18)$$

where S_y is the yield slope, S_v is the viscous slope, S_{td} is the turbulent-dispersive slope, τ_y is the Mohr Coulomb yield stress, γ_m is the specific weight of the sediment mixture, K is the resistance parameter ($K = 2,285$ for urban studies (Flo-2D 2012)), η is the Bingham dynamic viscosity, ω is the depth-averaged velocity, n is the Manning roughness coefficient.

Rheological properties, Bingham dynamic viscosity (η) and Mohr Coulomb yield stress (τ_y), are formulated as exponential functions of the sediment volume concentration (Julien and Leon 2000; Julien 2010). The yield stress and the dynamic viscosity are represented as

$$\eta = \alpha_2 e^{\beta_2 c_v} \quad (19)$$

$$\tau_y = \alpha_1 e^{\beta_1 c_v} \quad (20)$$

where c_v is the sediment concentration, α_i and β_i are empirical coefficients defined by laboratory experiment (Flo-2D 2009). Since we have very limited geological information for the study area, the values recommended by the Flo-2D manual for the empirical coefficients are used. Due to the steepness of the terrain and the low cohesion of the material forming the moraines (the main source of sediment for a GLOF), we expect high velocities and turbulent flows with dynamic viscosity on the order of the dynamic viscosity of water as well as low yield stress values (Julien and Leon 2000). Therefore, we have used empirical coefficients: $\alpha_1 = 0.0765$, $\beta_1 = 16.9$, $\alpha_2 = 0.0648$ and $\beta_2 = 6.2$, which give low values for the dynamic viscosity and yield stress similar to the list recommended in the Flo-2D manual (Flo-2D 2012). Dynamic viscosity and yield stress values are also functions of the sediment concentration. Lateral moraines are considered to be a major source of sediment for GLOFs in the Himalayan and Peruvian Andes (Huggel *et al.* 2004). According to Huggel *et al.* (2004), GLOFs generally have average concentrations by volume on the order of 50-60%. In modeling a previous event in Cordillera Blanca at Lake 513, Schneider

et al. (2014) used a sediment concentration by volume of 50%. In addition, Julien and Leon (2000) recommend using a concentration by volume of 50%, which also corresponds to the ranges given by Rickenmann (1999). Therefore, due to the lack of geological information, we use 50% concentration by volume, which results in a reasonable upper bound for the GLOF volume. We also run the model with different values of sediment concentration in order to estimate how sensitive the impacts at the city are to this parameter.

Although the geometry of the grid within the Flo-2D model is two dimensional, the flow is modeled in eight directions and it solves the one-dimensional equation in each direction. Each velocity computation is essentially one-dimensional in nature and is solved independently of the other seven directions. The continuity and momentum equations are solved with a central, finite difference method with an explicit time-stepping scheme, which uses a Courant-Friedrich-Lewy (CFL) condition for numerical stability.

Figure 11 shows the Paria River canyon (Quebrada Cojup) looking towards the outlet of the canyon and the City of Huaraz. Figure 12 shows five cross-sections where the flood hydrographs are computed. Figure 13 shows a close-up of the City of Huaraz and some of the features included in the flood simulation.



Figure 11. Paria River canyon (Quebrada Cojup) looking downstream.

3.6. Hazard Identification

Flood hazard is the result of the combination of probability and intensity of a flood event. Probability is also inversely related to the flood intensity since the probability decreases as the intensity of a flood increases. The intensity of an inundation is a function of the maximum depth and velocity of the flood (Table 3) (Garcia *et al.* 2002; García *et al.* 2003). The criteria listed in Table 3 were first proposed in the Venezuelan project PREVENE (2001) for the evaluation of the impacts of debris flow in two alluvial fans. Later this was adapted and applied to other alluvial fans in Venezuela (García *et al.* 2002). The methodology is an adaptation of the Austrian (Fiebiger 1997) and Swiss (OFEE *et al.* 1997) methodologies, in which García *et al.* (2002) assumed that the infrastructure in Venezuela is less resistant than the infrastructure in Austria or Switzerland. This is important since the city of Huaraz is more similar to a city in Venezuela than a city in Europe in terms of building resistance. This methodology consists of the classification of areas inundated with water or debris flow into three hazard levels (low, medium, and high). The classification criteria are shown in Table 3 for debris flows since that is the most probable case for a GLOF from Lake Palcacocha. Note that we do not consider the very low hazard level (depth less than 0.2 m). A low level of hazard is present when depths are small and the discharge per unit width is small. The medium hazard level is present when the depths and discharge are at medium levels. The high hazard level is present when the depth is high or the discharge is high, or both.

Other hazard identification systems for debris flows could be used, but we present just one example, based on the Swiss and Venezuelan experience. Also, we have not defined the very low and very high hazard levels that are sometimes defined in other methods. Vulnerability of the population or infrastructure is not considered here, just the physical hazard level of the events modeled.

Table 3. Debris Flow Event Hazard Level.

Hazard Level	Description	Flow Depth h (m)		Discharge per Unit Width $v * h$ (m²/s)
Low	People at low risk. Minor damage to buildings.	$0.2 < h < 1.0$	and	$v * h < 0.2$
Medium	People in danger outside their homes. Structural damage and possible destruction.	$0.2 < h < 1.0$	and	$0.2 < v * h < 1.0$
High	People in danger inside and outside homes. Structures destroyed.	$h > 1.0$	or	$v * h > 1.0$

4. RESULTS

4.1. Avalanche Simulation

The results of the avalanche simulations are shown in Table 4. The RAMMS model simulation period was 60 seconds. In all three scenarios the avalanches reach Lake Palcacocha after 35-38 seconds. For all three scenarios, 100% of the mass released reached the lake. The results of the avalanche simulations provide the input conditions for the lake wave simulations.

Table 4. Characteristics of RAMMS Simulated Avalanches for Three Scenarios.

Avalanche Scenario	Volume (10⁶ m³)	Thickness at Lake Entry (m)	Velocity at Lake Entry (m/s)
Small	0.5	6	20
Medium	1.0	15	32
Large	3.0	20	50

4.2. Lake Simulation

As the avalanche impacts the lake, it generates a large wave that propagates lengthwise along the lake towards the terminal moraine and reaches its maximum height when it has traveled approximately one third of the length of the lake. The maximum wave height is only slightly attenuated as it propagates across the lake, resulting in a significant amount of water overtopping the terminal moraine. The overtopping results in a sharp peak in the outflow hydrograph from the lake. The total time from the avalanche initiation to the peak overtopping discharge from the lake is approximately 2 minutes.

The wave characteristics calculated according to the Heller *et al.* (2009) empirical method are presented in Table 5. The key characteristics of modeling the large scenario wave in Flow-3D are presented in Table 6. Only the results from the hydrodynamic model of the large avalanche scenario are presented here because the large scenario is a reasonable representation of the worst-case scenario and can be used for decision-making purposes. Images showing the fluid depth for the simulation of the large scenario at several key points are shown in Figure 12-14. The overtopping hydrograph for the large avalanche scenario is shown in Figure 15.

Table 5. Waves Calculated for Three Avalanche Scenarios Using Empirical Method.

Avalanche Scenario	Maximum Wave Height (m above initial free surface)	Distance to Maximum Wave Height (m)
Small	9	147
Medium	21	254
Large	42	392

Table 6. Waves Calculated for Large Avalanche Scenario Using Flow-3D Model.

Item	Value
Maximum Wave Height (m above initial free surface)	35
Peak Discharge of Overtopping (m ³ /s)	5.3x10 ⁴
Total Volume of Overtopping (m ³)	2.5x10 ⁶

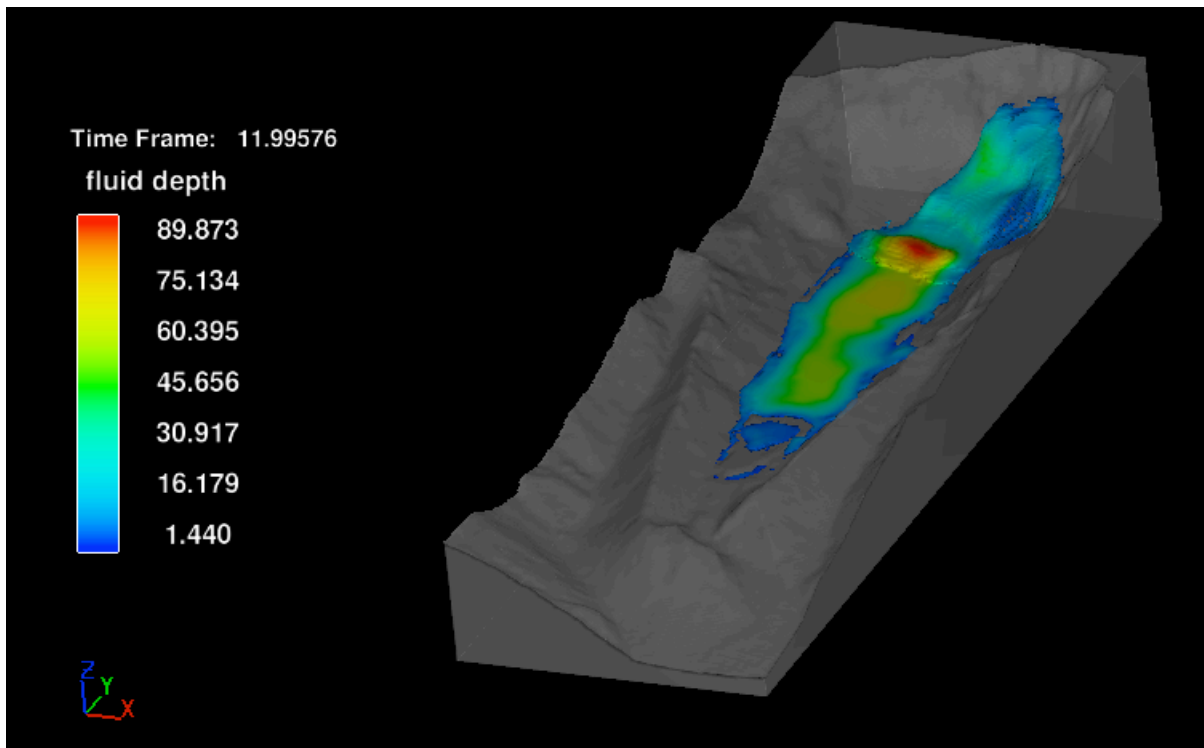


Figure 12. Wave for the large avalanche scenario represented by fluid depth just after the avalanche enters the lake

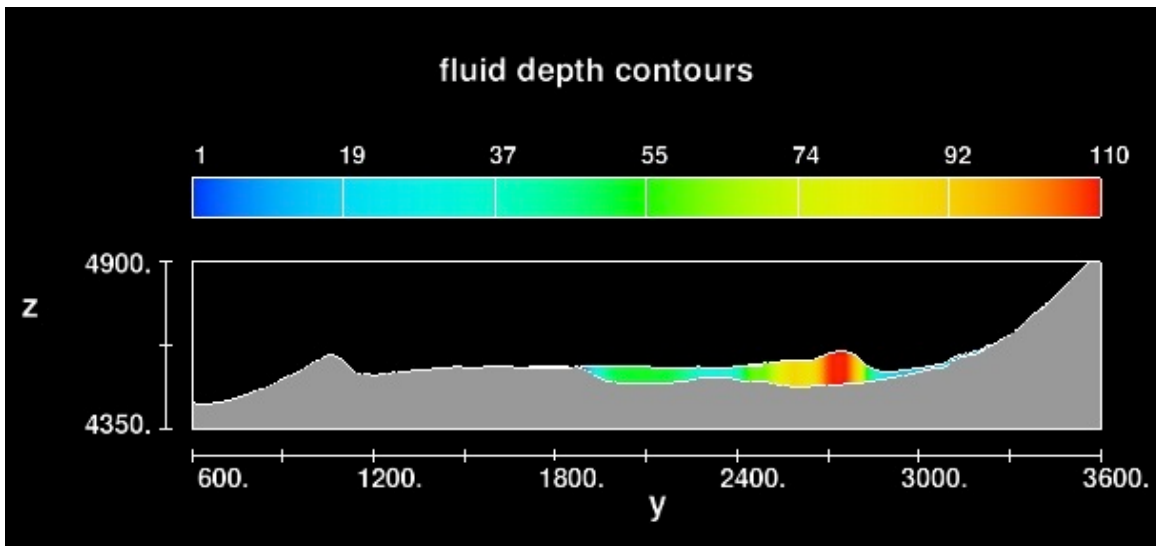
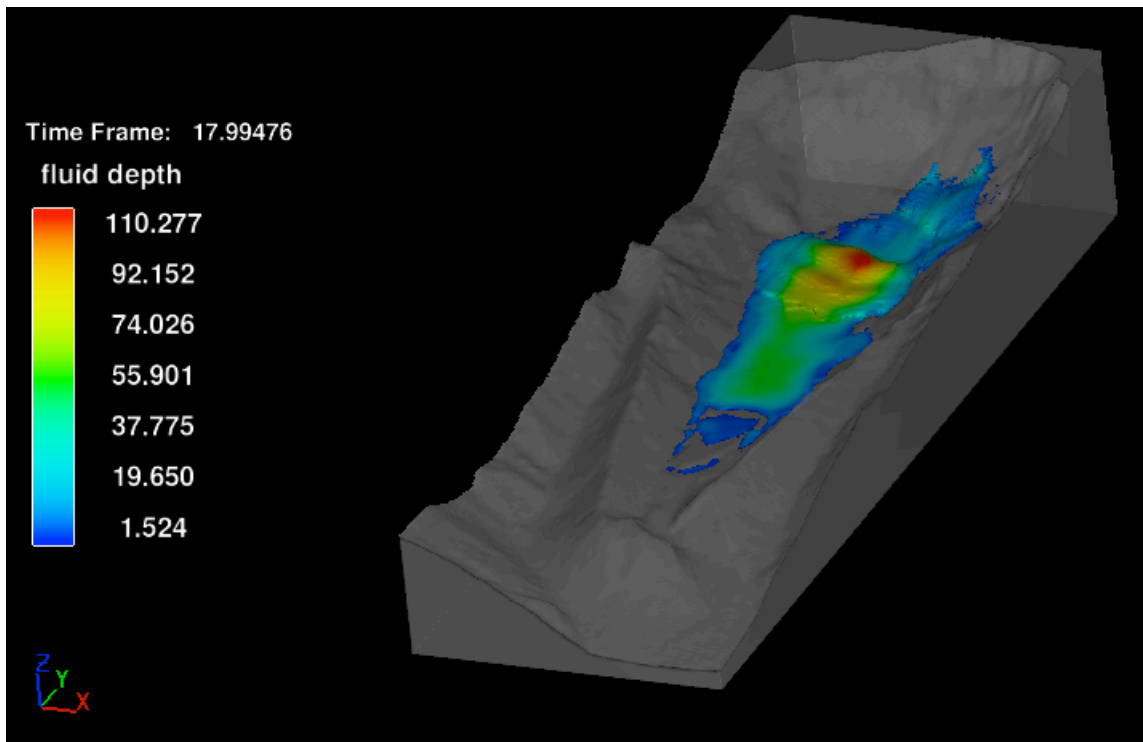


Figure 13. Wave for the large avalanche scenario at its maximum height: (top) orthographic view and (bottom) wave profile

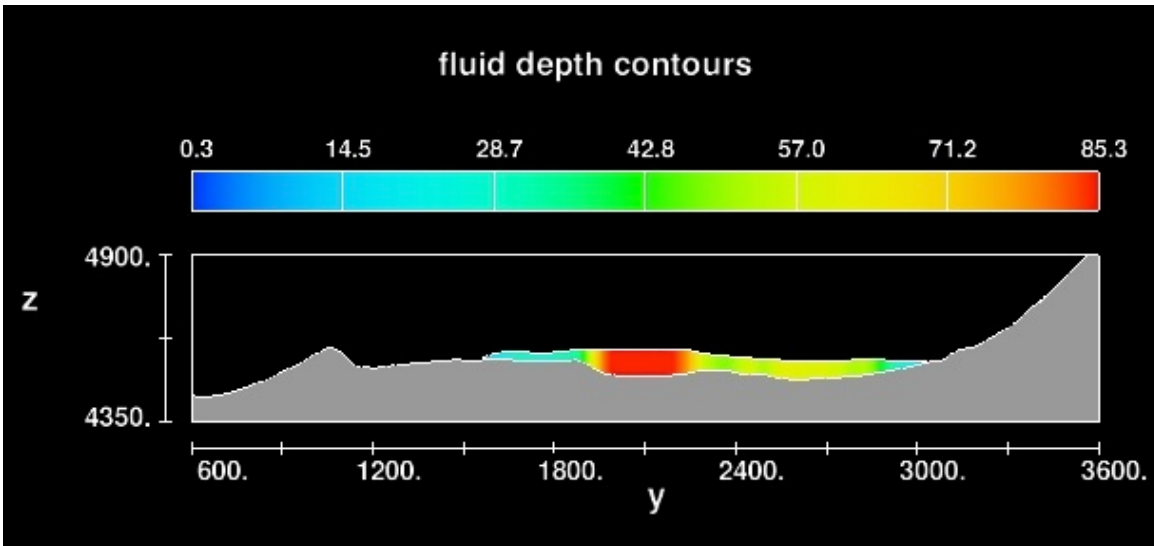
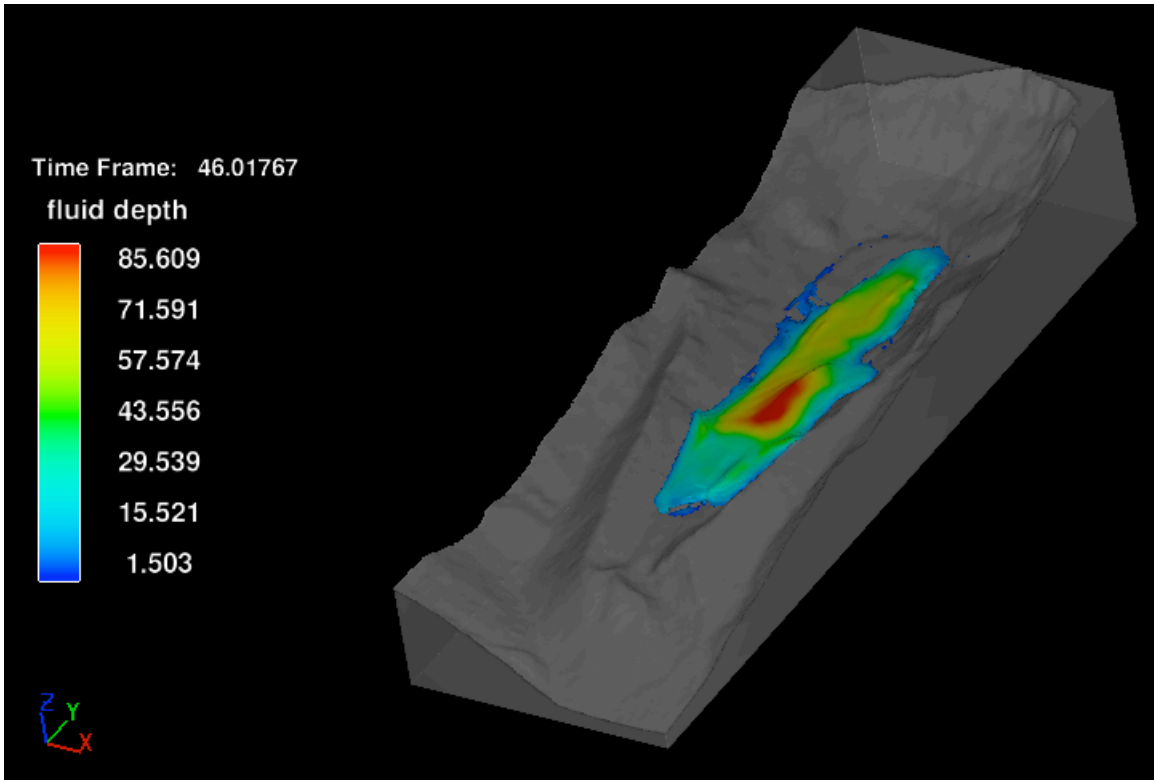


Figure 14. Wave for the large avalanche scenario at the point of overtopping the terminal moraine: (top) orthographic view and (bottom) wave profile

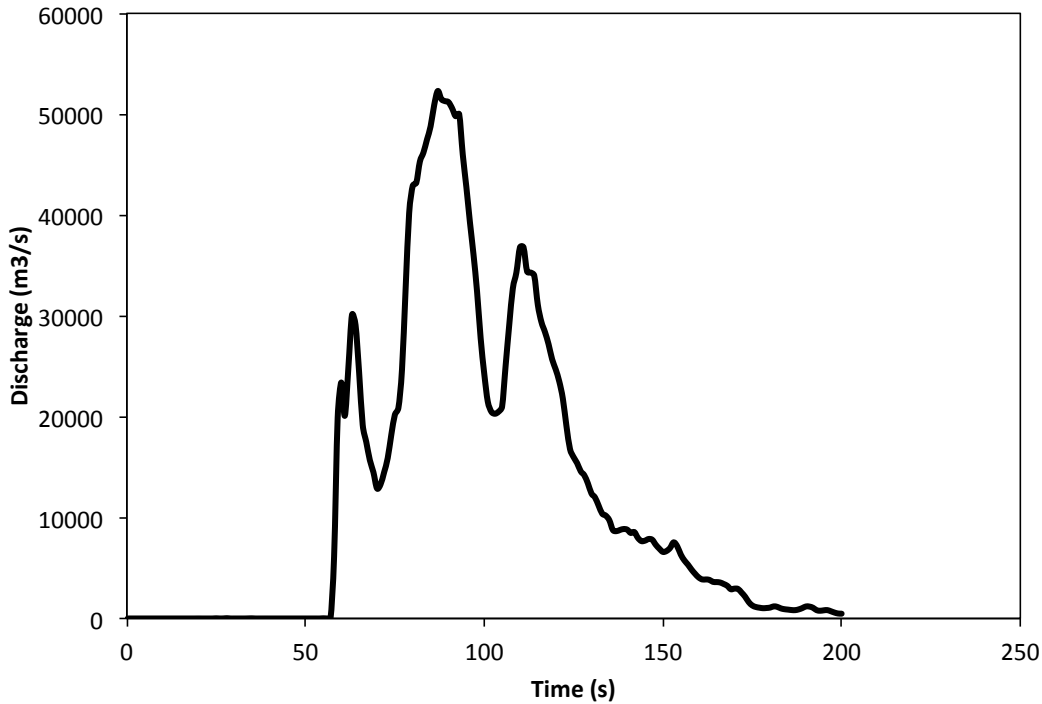


Figure 15. Hydrograph of discharge at the lake outlet due to wave overtopping for the large avalanche scenario.

4.3. Moraine Breach Simulation

Discharge hydrographs from Lake Palcacocha were generated for the breaching of the moraine using MIKE-11. Figure 16 shows the outflow hydrographs corresponding to the cases where the breach depth reaches 56 m and 22.5 m, respectively. Low flow events are more likely to occur because the shallower layers of the moraine are more susceptible to erosion (less surface area and less material cohesion under self-pressure). The 22m-breach hydrograph ($Q_p = 5528 \text{ m}^3/\text{s}$ at 32 min) coincides with the lower bound of the confidence interval given by the empirical Froehlich model. When the wave overtopping hydrograph is combined with the moraine breach hydrograph, the resulting combined hydrograph of the GLOF is determined as shown in Figure 17.

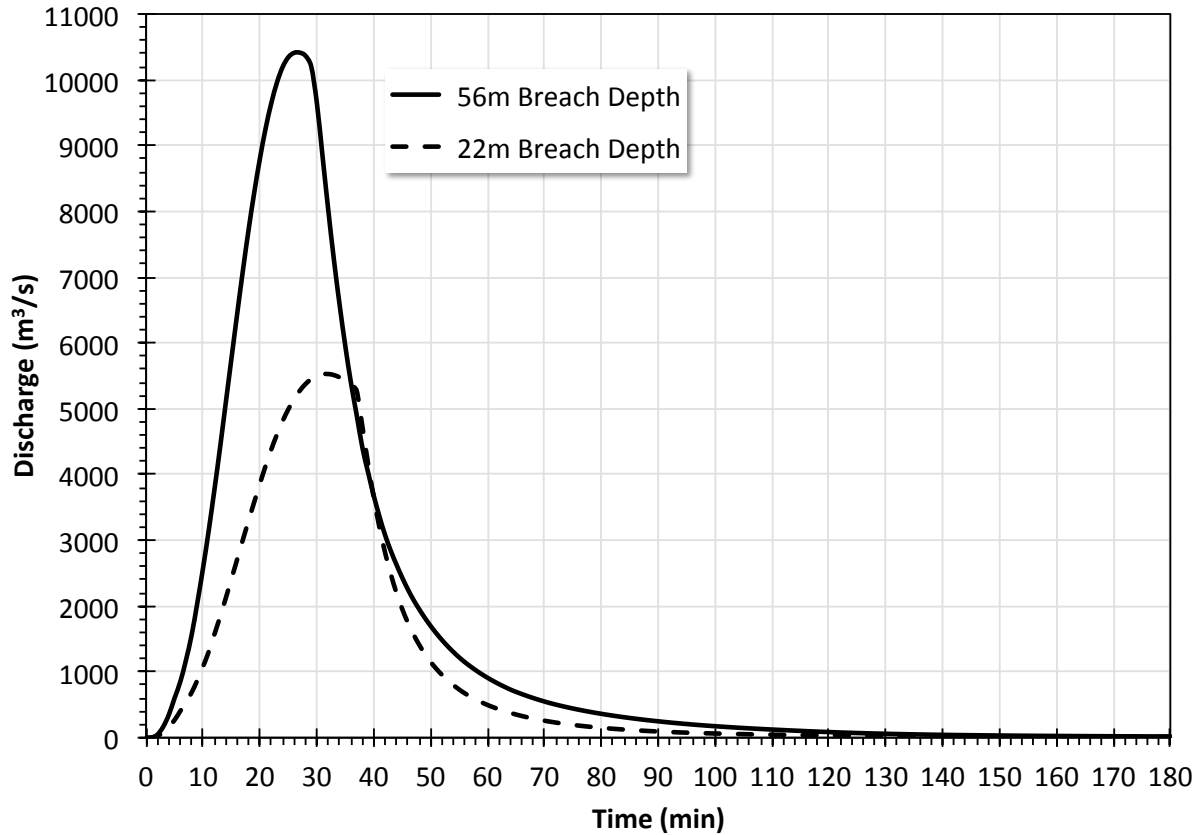


Figure 16. Maximum and minimum potential outflow hydrographs from Lake Palcacocha due to a moraine breach.

Combining the wave-overtopping hydrographs with the moraine erosion hydrograph results in the combined hydrographs for the 22.5 and 56 m breaches (Figure 17). These hydrographs represent two consecutive processes of different nature and scale. While the outflow from the wave-overtopping event is almost instantaneous, the erosive moraine failure takes more than one hour to drain most of the lake’s water. Both phenomena pose different kinds of hazards: the destructive power of a relatively small volume of water released at extremely high velocities in the case of the overtopping wave that helps to initiate the moraine erosion, and the more sustained effect of the much larger volume drained by the moraine breach. The impacts of this combined hydrographs on downstream floods is explored in the next section.

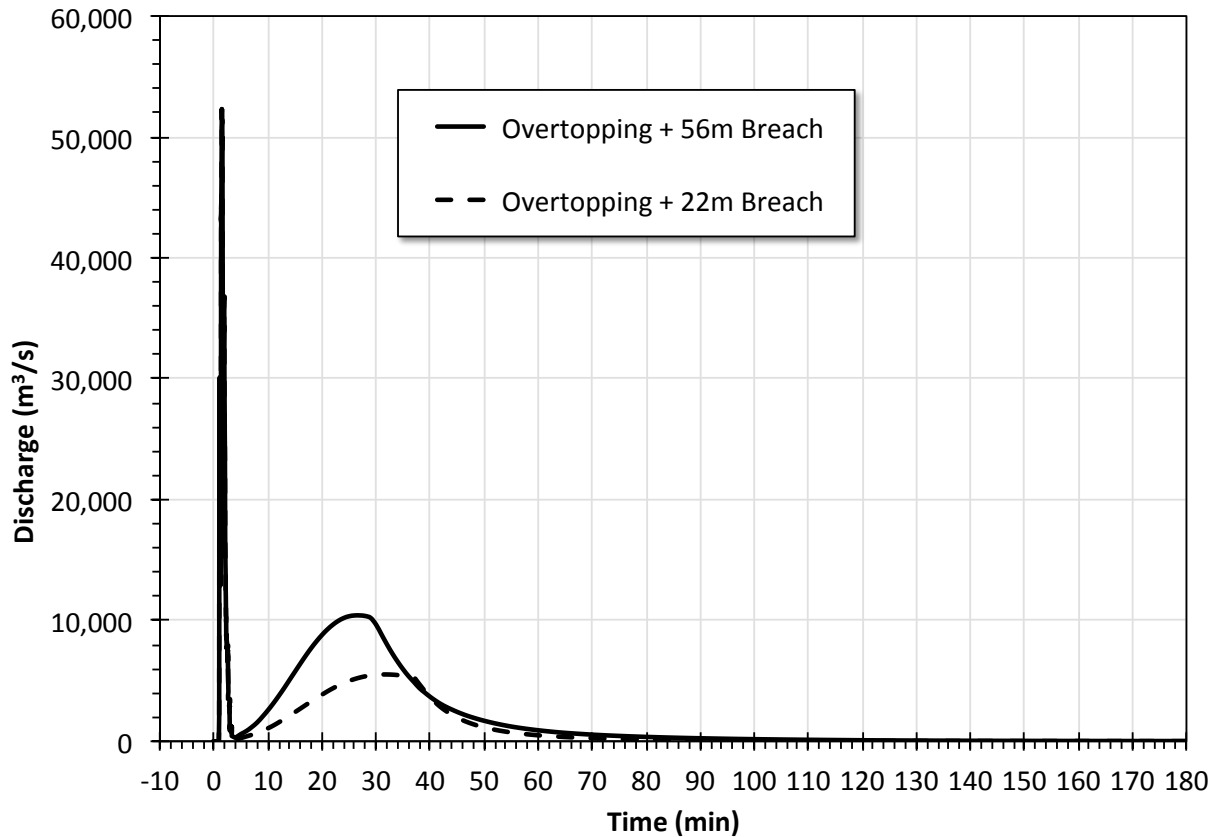


Figure 17. Combined wave overtopping and 56m and 22m breaching hydrographs.

4.4. Inundation Simulation

Figure 18 shows the locations of the five cross-sections downstream of Lake Palcacocha where flood hydrographs from the Flo-2D simulations are reported. Table 7 provides details of the locations of the cross-sections. Figures 19 and 20 show the hydrographs at the five cross-sections downstream of Lake Palcacocha resulting from the 56 m and 22.5 m breach scenarios, respectively. Table 8 provides details of the results at the cross-sections. At cross-section 1 the hydrograph is still similar to the original hydrograph at the lake with the overtopping-wave hydrograph preceding the moraine erosion hydrograph. The hydrograph at cross-section 2, located just upstream of the point where the Paria River canyon (Quebrada Cojup) narrows and becomes steeper, shows that the flow from the moraine erosion and lake discharge catches up to the overtopping flood wave; at this point the volumes from the two events mix and continue downstream as one event. This is expected because the river is relatively wide with gentle slopes between the lake and the second cross-section, and in this reach the maximum velocity is only 2-

4 m/s. Sediments eroded from the moraine would be deposited in this section before the flood continues downstream. Cross-section 3 is located at the entrance to the Huascarán National Park where the large moraines will supply sediment to the inundation starting at this point. In addition, villages start appearing below this point increasing people’s exposure to the GLOF.

Cross-section 4 is located at the entrance to the city. From the beginning of the avalanche event it takes slightly more than one hour for the 56 m breach flood to reach this location and 1.2 hours for the 22.5 m breach to reach that location. The hydrograph peaks diminish about 10% between the second and fourth cross-sections. The biggest changes in slope occur between cross-sections 3 and 4, when the flow accelerates; as a consequence the flow is able to scour the large lateral moraines in this reach adding to the volume of sediments in the flood. The hydrograph at cross-section 5 shows the peak discharge in the Rio Santa exiting the city. The peak has attenuated considerably at this point. The flood arrives at this cross-section after about 1.3 and 1.6 hours for the 56 m and 22.5 m breach events, respectively. The peak flow takes about 30 minutes to cross the city.

Table 7. Location of Flood Hydrograph Cross-sections Downstream of Lake Palcacocha

Section	Latitude (deg)	Longitude (deg)	Elevation (m)	Distance to Lake Outlet (m)
1	-9.4200	-77.3900	4,313	1,912
2	-9.4605	-77.4292	4,052	8,319
3	-9.4831	-77.4516	3,774	11,886
4	-9.5264	-77.5040	3,165	20,177
5	-9.5039	-77.5373	2,965	26,517

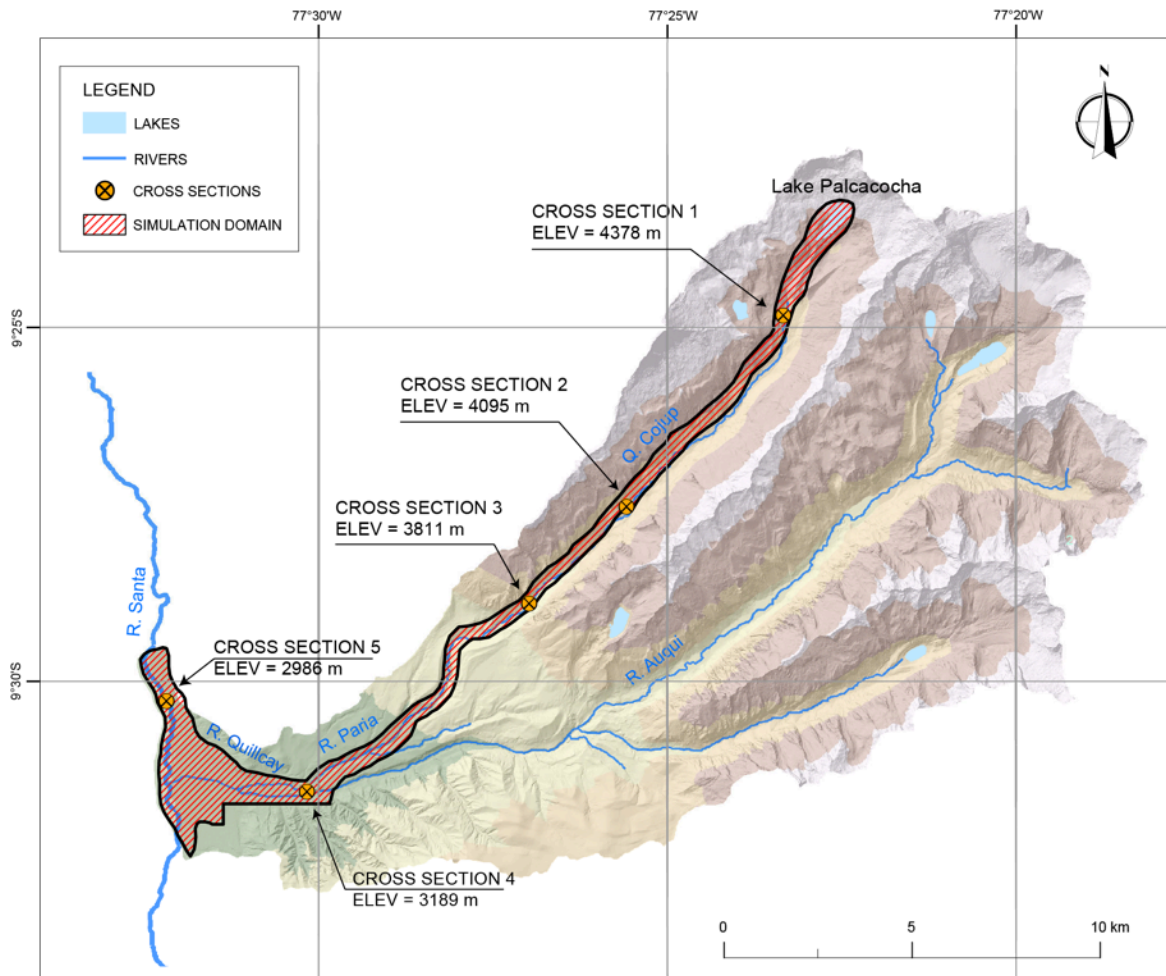


Figure 18. Cross-sections for FLO-2D Simulation Results.

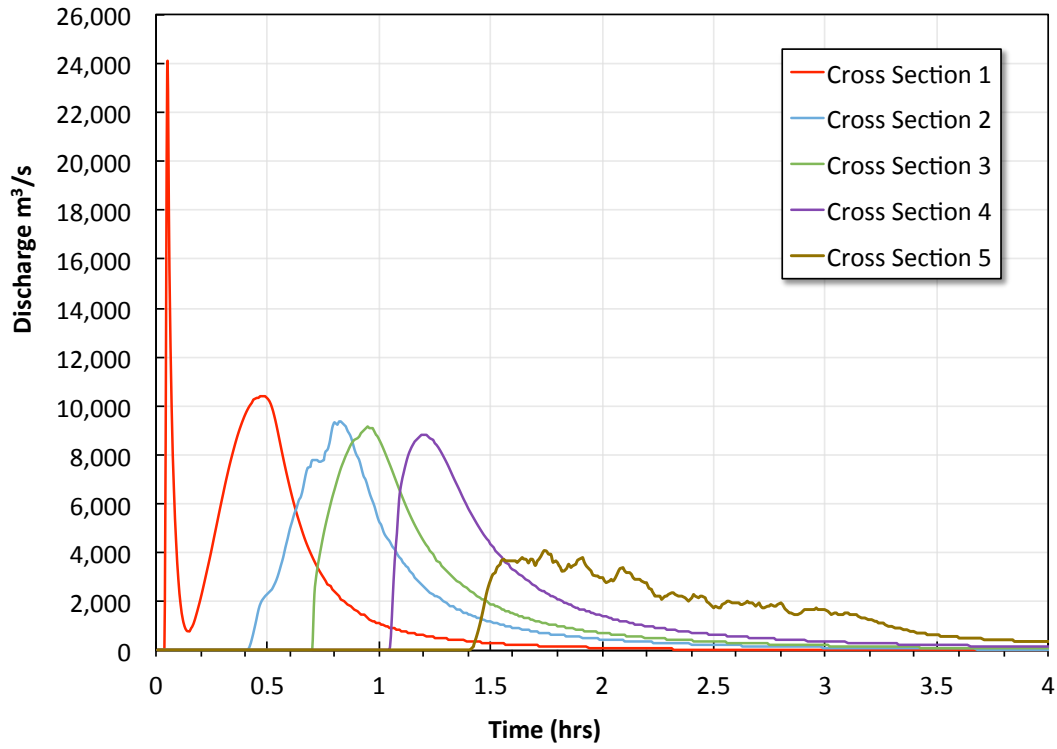


Figure 19. Hydrographs at cross-sections for the 56 m breach event.

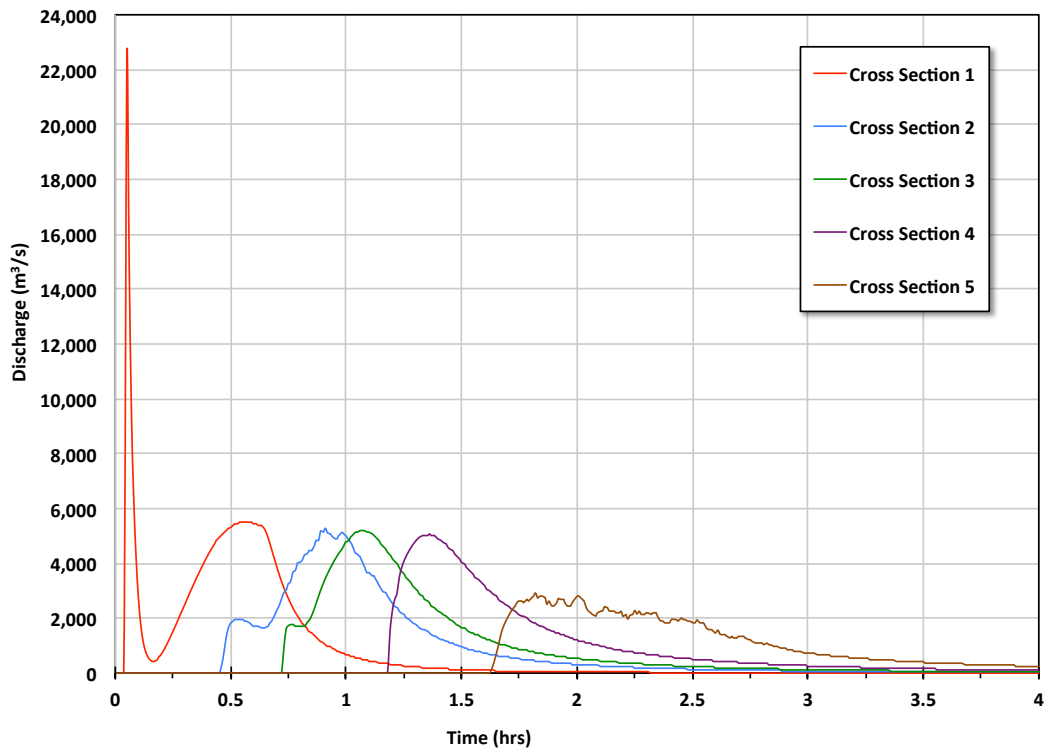


Figure 20. Hydrographs at cross-sections for the 22.5 m breach event.

Table 8. Flo-2D Simulation Results at Cross-sections Downstream of Lake Palcacocha

Section	Arrival Time (hr)	Peak Time (hr)	Peak Discharge (m³/s)	Total Volume (10⁶ m³)
56 m breach				
1 - Overtopping wave	0.05	0.05	23,657	2.4
1 - Moraine erosion	0.17	0.48	10,387	17.4
2	0.47	0.85	9,351	19.8
3	0.71	0.95	9,138	19.7
4	1.06	1.2	8,822	19.5
5	1.42	1.75	4,091	18.6
22.5 m breach				
1 - Overtopping wave	0.05	0.05	22,299	2.37
1 - Moraine erosion	0.21	0.57	5,507	10.12
2	0.5	0.91	5,280	12.28
3	0.74	1.07	5,190	12.16
4	1.21	1.38	5,048	11.76
5	1.63	1.84	2,840	10.71

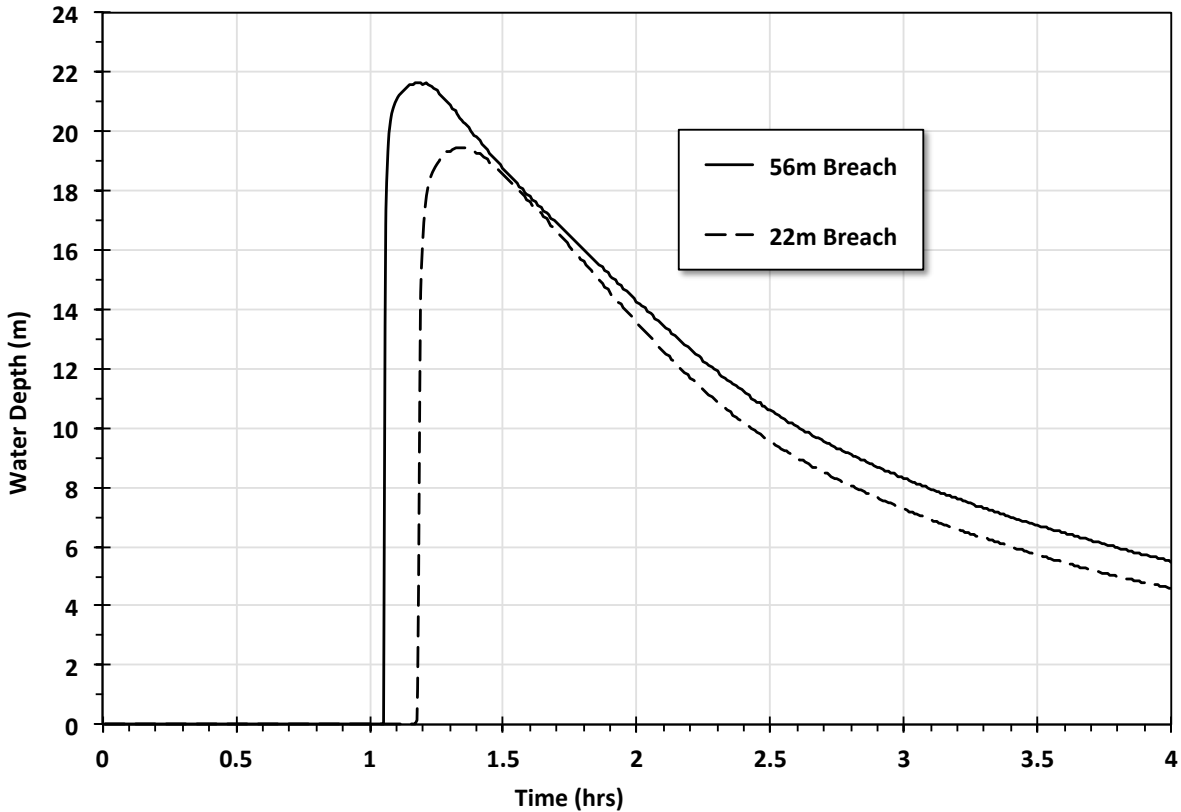


Figure 21. Flood depth versus time at cross-section 4 for the 56 m and 22.5 m breach events.

4.5. Inundation in Huaraz

The resulting maximum flood depth within Huaraz for the 56 m and 22.5 m events are shown in Figures 22 and 23, respectively. The deepest areas are near the existing channels of the Quillcay River and the Rio Santa. The highest inundation depths occur at the south side of the river, where most of the commerce is located in Huaraz. Considering the 56 m breach event, within the city, the area where the depths are small (<1 m) is limited to 0.13 km² in a narrow band ranging from 20 to 60 meters in width along the outskirts of the flooded area. The area flooded to a depth between 0.2-1 m covers an area of 0.51 km² and the area flooded to depths greater than 1 m covers an area of 4.5 km². The area near the channel of the Quillcay River shows depths of 5-10 m in a band approximately 350 m wide in the east side of the city and up to 500 m wide in the west side of the city near the Santa River. In comparing the two events, one can see that areas that had inundation depths of 1-2 m in the 56 m breach have depths of 0.1-1 m

in the 22.5 m event. Likewise areas that show 4-6 m depth in the 56 m event reduce to 3-4 m depth in the 22.5 m event, and 8-10 m depth areas reduce to 6-8 m depth in the 22.5 m breach event.

The maximum velocities within the city are shown in Figures 24 and 25 for the 56 m and 22 m events, respectively. Similar to the inundation depths, the maximum velocities occur along the channels of the Quillcay River and the Rio Santa. Considering the 56 m breach event, within the city, velocities in excess of 8 m/s (red in Figure 24) occur only in the narrow river channel in the canyon and in small isolated areas in the city. Velocities between 5-8 m/s (yellow) occur in the areas where the inundation depths are between 5-10 m. In the outer area velocities of 0-2 m/s (blue and light blue) occur in areas with depths lower than 5 m. Velocity reductions for the 22.5 m breaching event, compared to the 56 m event, follow the same pattern as the inundation depths discussed above.

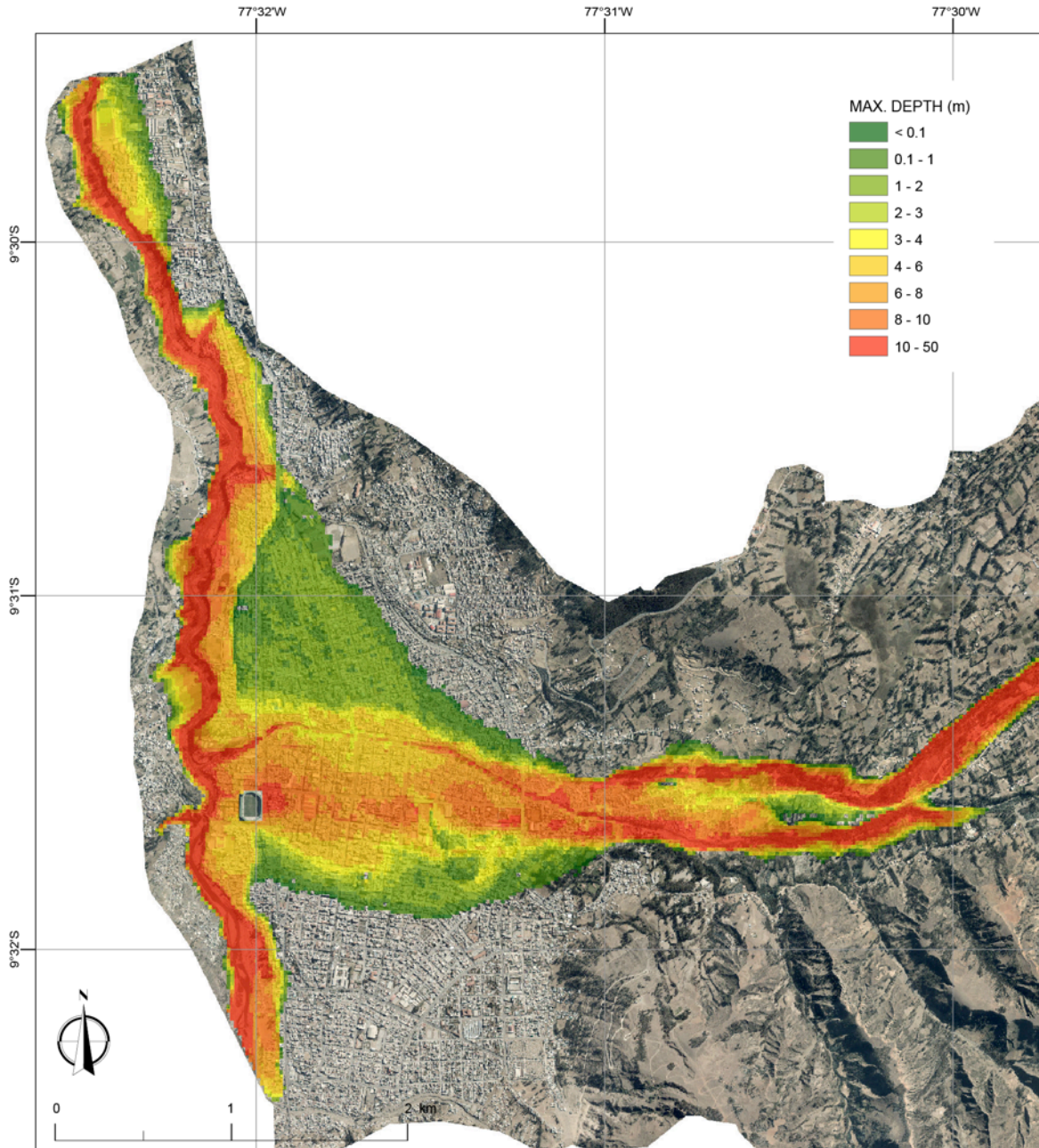


Figure 22. Water depth from GLOF inundation in Huaraz from combined hydrograph for 56 m breach event.

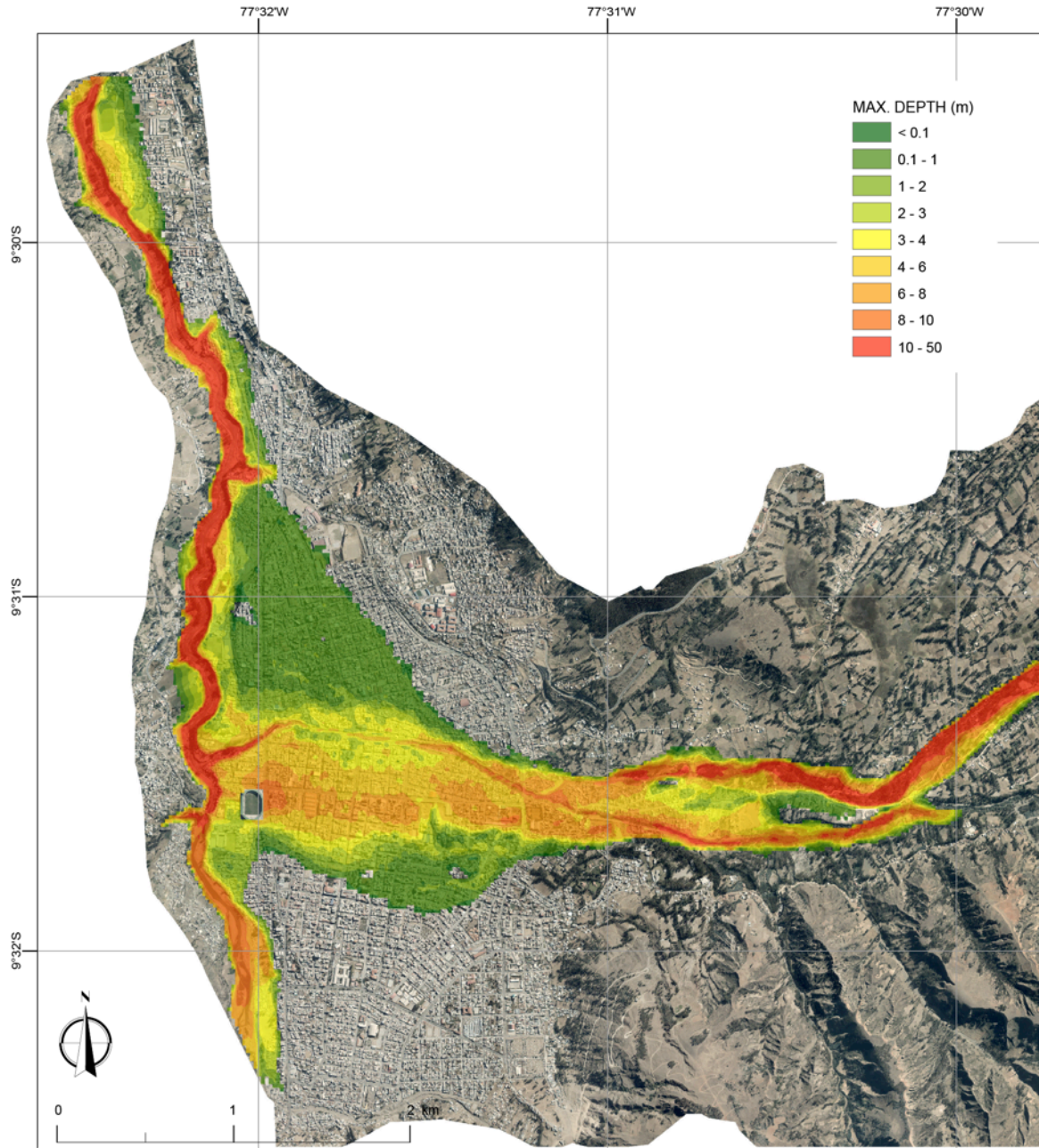


Figure 23. Water depth from GLOF inundation in Huaraz from combined hydrograph for 22 m breach event.

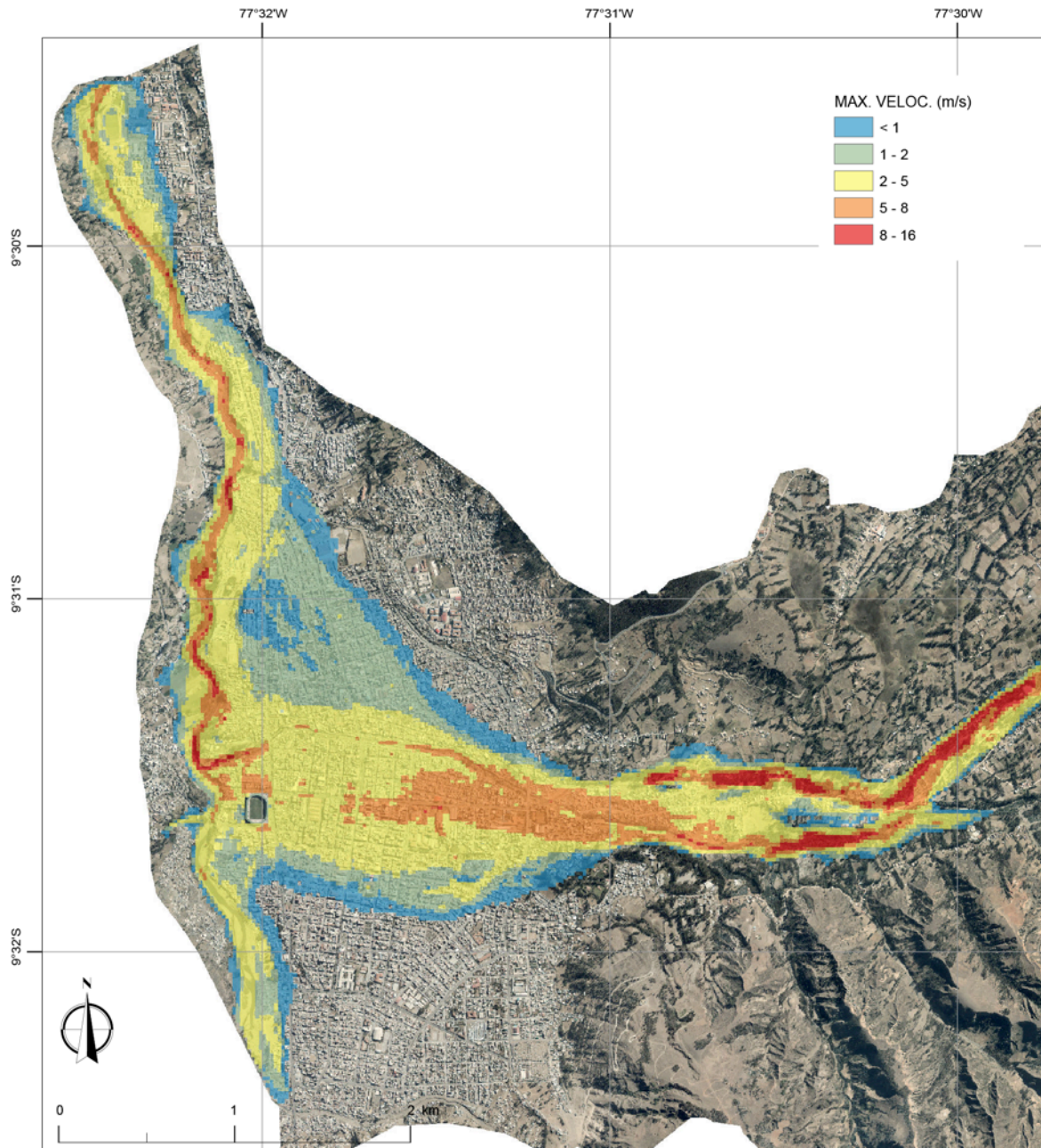


Figure 24. Maximum velocity of the flood waters in Huaraz for the large avalanche scenario for 56 m breach event.

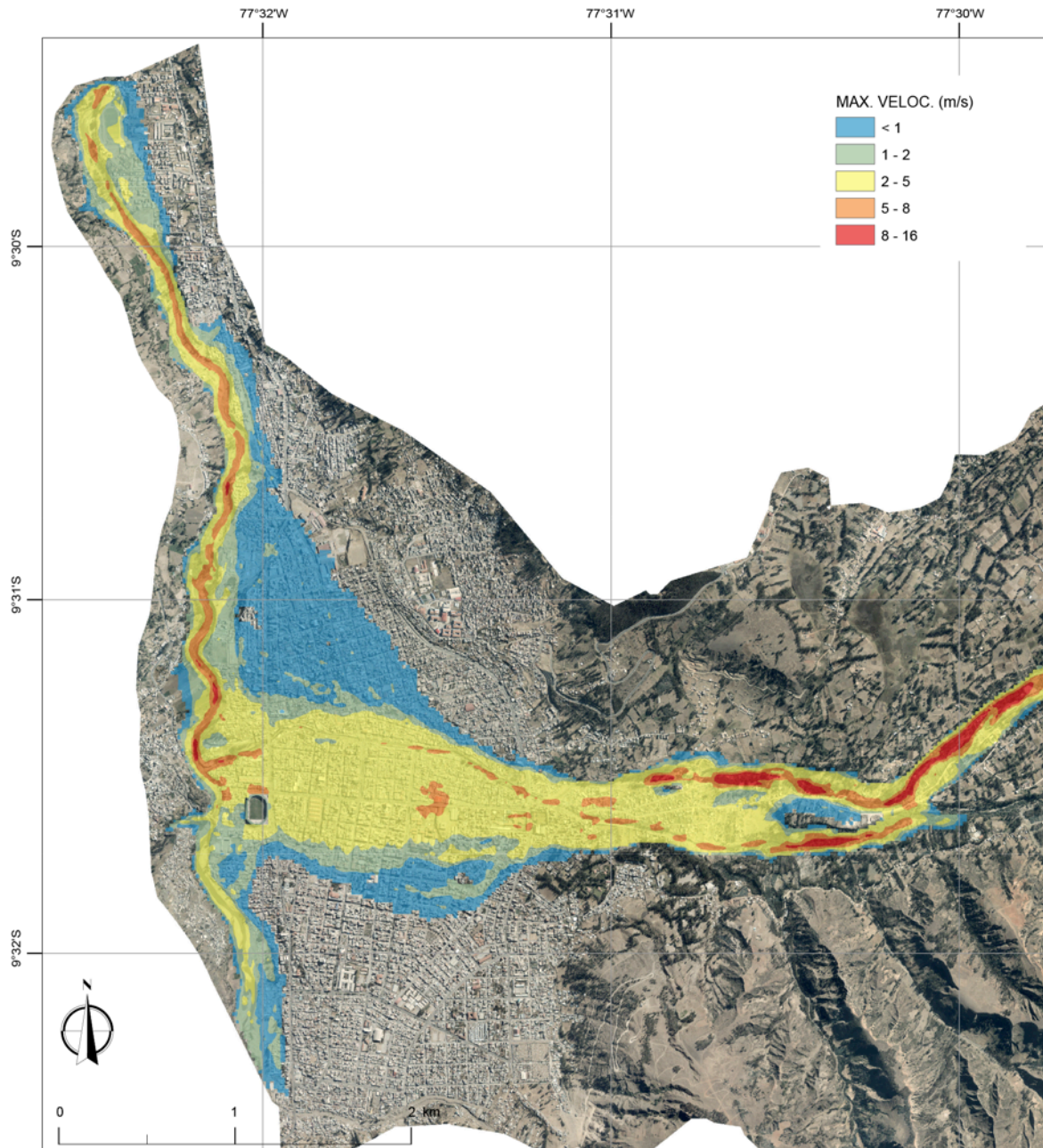


Figure 25. Maximum velocity of the flood waters in Huaraz for the large avalanche scenario for 22 m breach event.

4.6. Hazard Identification

The hazard identification method described in the previous section, using the maximum inundation depth and the maximum water velocity, is used to determine the level of hazard at

different points in the city. Figures 26 and 27 show the computed hazard levels for the 56 m and 22 m events, respectively. As shown in Figure 26, almost all of the inundated areas within the city are in the high hazard zone (red) for the 56 m event. Very small areas on the fringe of the flooded area are in the medium (yellow) or low (green) hazard zones. For the 22.5 m event there is a reduction of the high (red) hazard zone and increase in the medium (yellow) hazard zone to the north of the Quillcay River.

The hazard methodology is based on the inundation intensity and it does not consider the time that people have to escape from the hazard zone. In Figures 28 and 29 show how the inundation progresses in the city for the 56 and 22.5 m events, respectively. For the 56 m event about 1 hour after the avalanche induced wave occurs at the lake the flood arrives at the city and the maximum peak arrives 6 to 8 minutes later. Additionally the inundation crosses the city from east to west in around 20 minutes expanding to the north and south as it progresses through the city. This is similar for the 22.5 m breaching event but the flood is delayed by about 10 minutes.

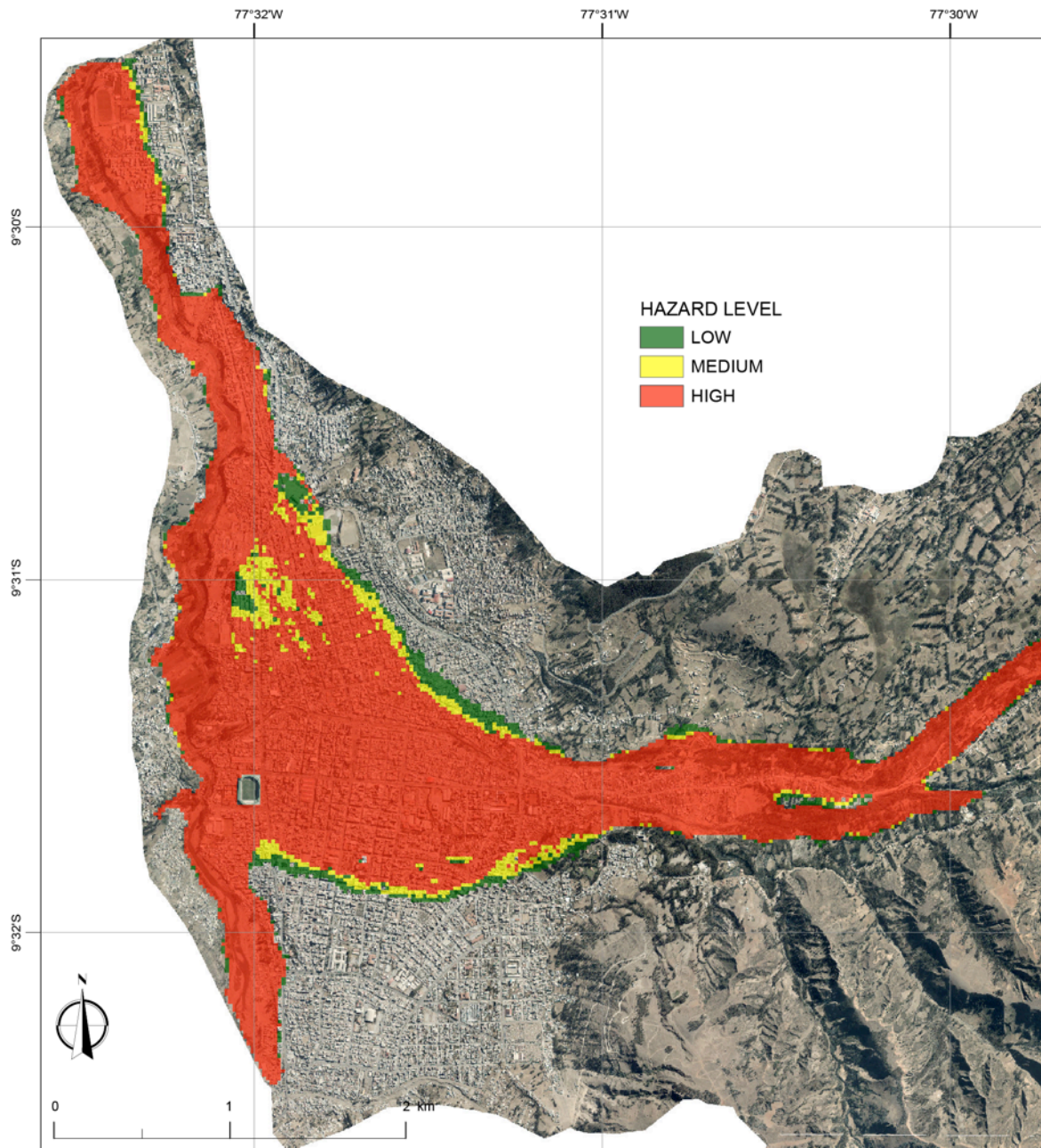


Figure 26. Hazard level in Huaraz from Lake Palcacocha GLOF for large avalanche scenario for the 56 m breaching event.

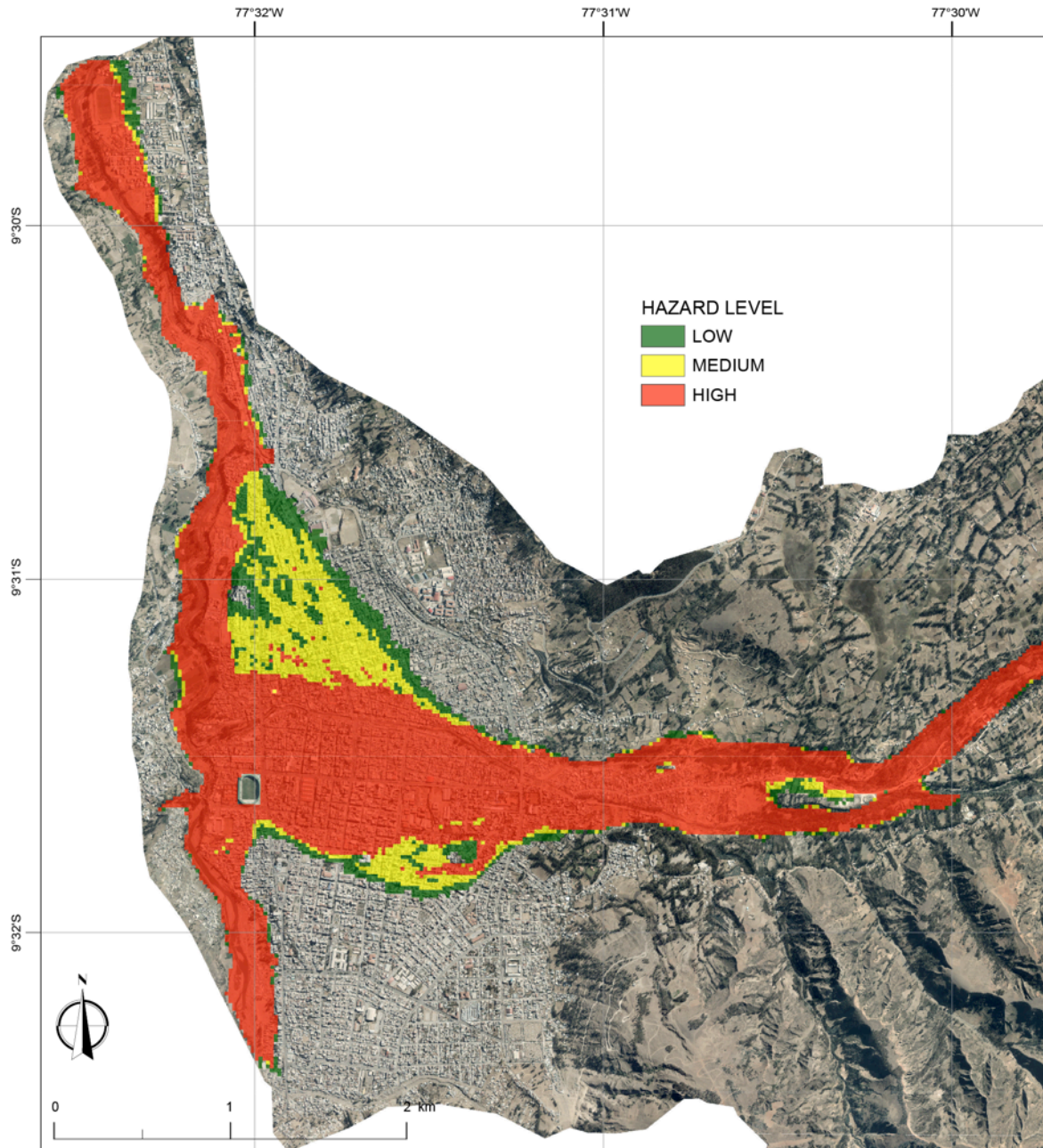


Figure 27. Hazard level in Huaraz from Lake Palcacocha GLOF for large avalanche scenario for the 22 m breaching event.

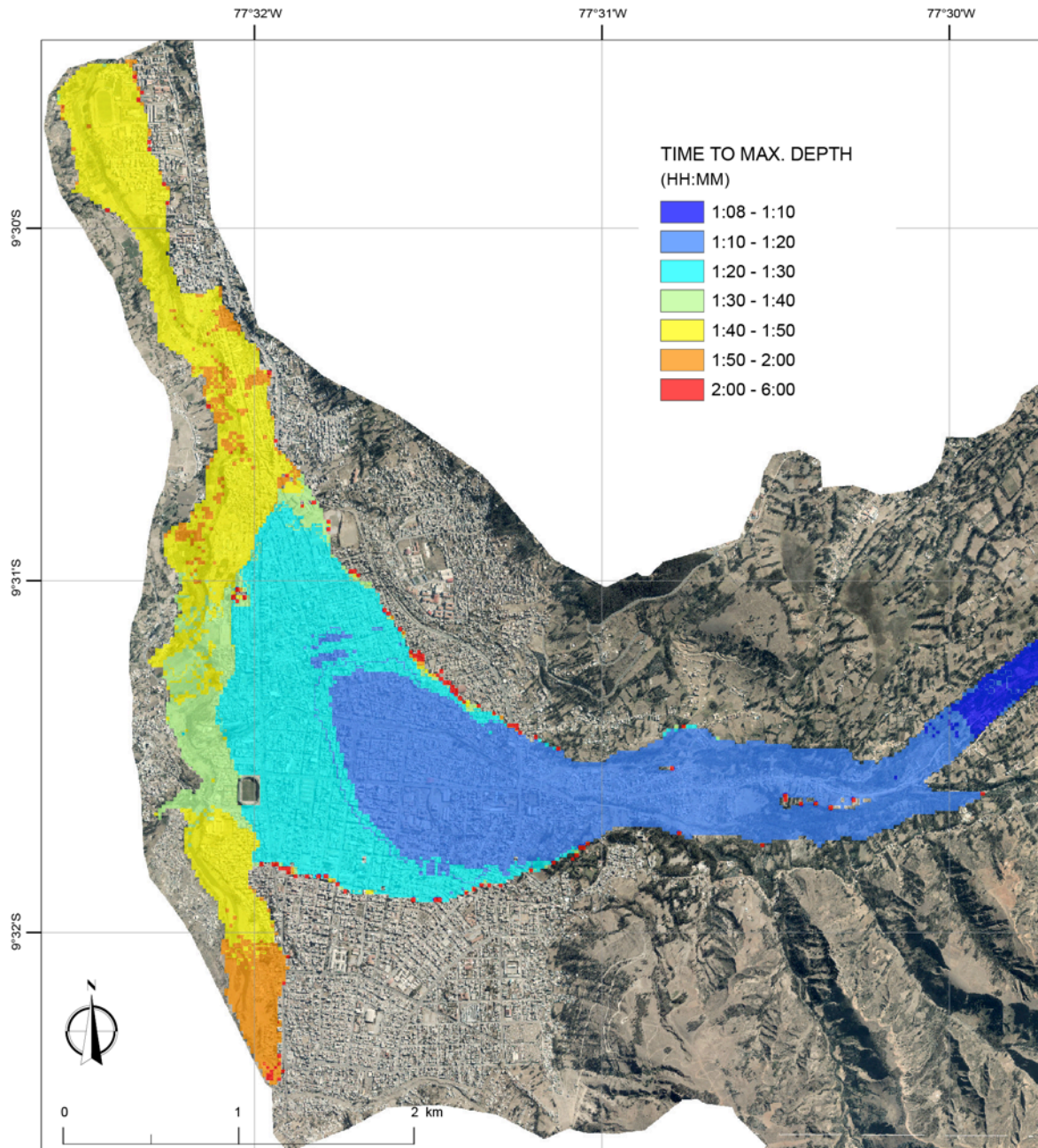


Figure 28. Time to maximum flood depth for the large avalanche scenario for the 56 m breaching event.

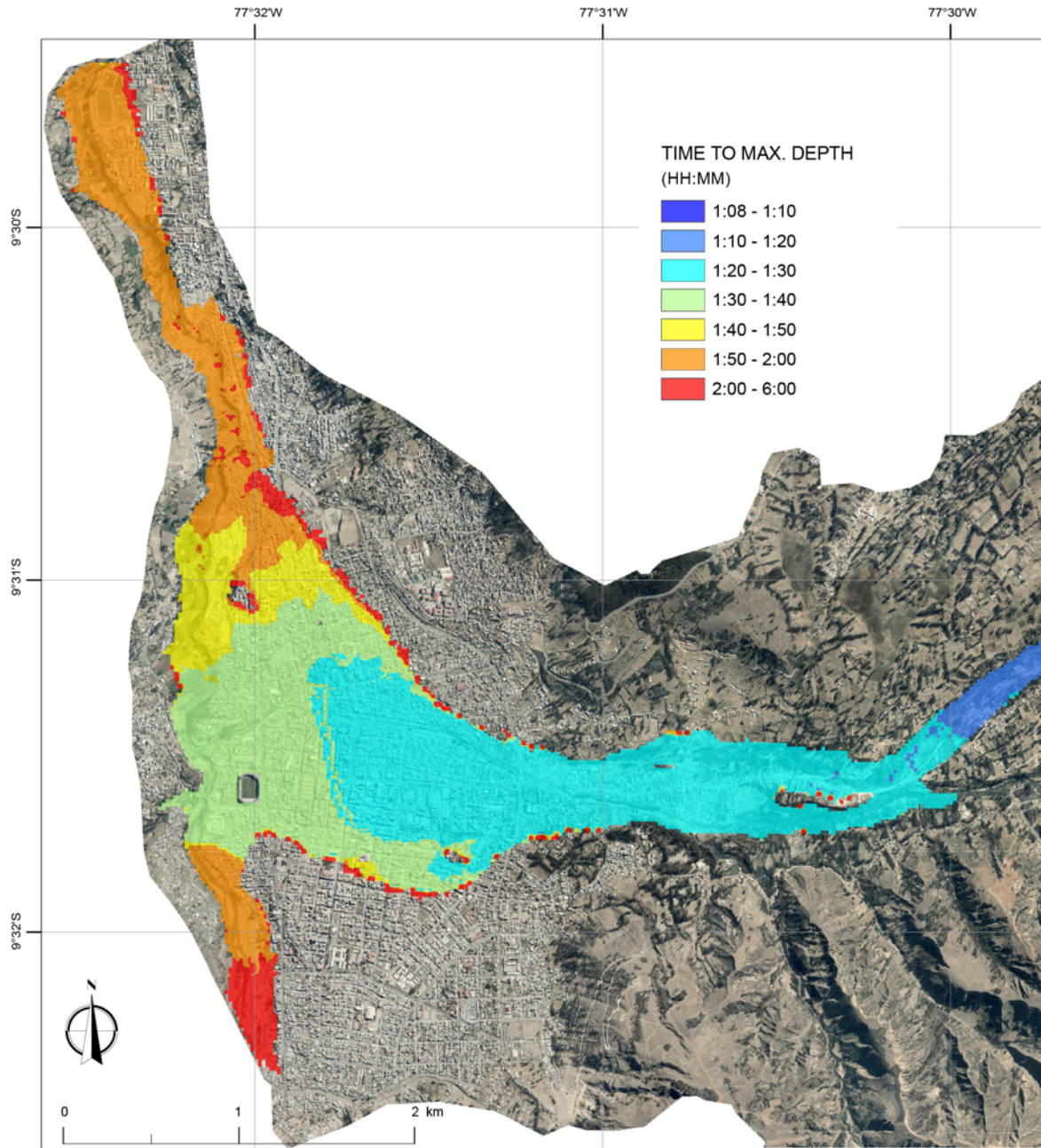


Figure 29. Time to maximum flood depth for the large avalanche scenario for the 22 m breaching event.

5. CONCLUSIONS

The chain of processes triggered by an avalanche into Lake Palcacocha in Peru were simulated to assess the level of hazard for the City of Huaraz. Avalanche simulations were carried out to determine the height and velocity of the avalanche material entering the lake and it

showed an avalanche height of 20m and a velocity of 50 m/s entering the lake. A three-dimensional hydrodynamic lake model was used to simulate the movement of the resulting impulse wave across the lake and the overtopping of the terminal moraine. The overtopping wave discharge hydrograph released a volume of $2.4 \times 10^6 \text{ m}^3$ of water. The moraine erosion resulting from the overtopping was simulated to provide a combined hydrograph of the released water and debris. Two scenarios of moraine erosion were simulated: a worst-case event of a 56 m breach and a smaller 22.5 m erosion event. The combined discharge hydrograph released a volume of $19.8 \times 10^6 \text{ m}^3$ for the 56 m event and $12.3 \times 10^6 \text{ m}^3$ for the 22.5 m event. These hydrographs were used as input to a two-dimensional flood model (water and debris), and the hydrographs was routed downstream reaching the City of Huaraz 1.06 and 1.20 hours after the avalanche for the 56 m and 22.5 m events, respectively. The inundation in the city is extensive in both breaching events with depths exceeding 1 m in many areas, especially near the channel of the Quillcay River, and the velocity of the flood exceeding 1 m/s in most of this area. Because of the inundation depth and the velocity of the flow, most of the area of the city that experiences flooding will have a very high hazard level, putting both lives and property at risk.

ACKNOWLEDGEMENTS

The authors acknowledge the support of the USAID Climate Change Resilient Development (CCRD) project and the Fulbright Foundation for the support of Somos-Valenzuela and Rivas. The support of the software developers of FLO-2D, FLOW3D, and RAMMS made much of the work reported here possible. The support of Josefa Rojas and Ricardo Ramirez Villanueva of the IMACC project of the Peruvian Ministry of Environment provided valuable assistance in obtaining the new DEM of the Quillcay watershed. Ing. Cesar Portocarrero, Prof. Wilfred Haerberli, Dr. Alton Byers and Dr. Jorge Recharte provided valuable insights and encouragement through the entire work.

REFERENCES

Ball, G.H. and D.J. Hall (1965) ISODATA, a Novel Method of Data Analysis and Pattern Classification. Stanford Research Institute, Menlo Park, Ca.

- Bartelt, P., Y. Buehler, M. Christen, Y. Deubelbeiss, M. Salz, M. Schneider, L. Schumacher (2013) RAMMS: Rapid Mass Movement Simulation: A numerical model for snow avalanches in research and practice. User Manual v1.5 – Avalanche. Swiss Federal Institute for Forest, Snow and Landscape Research WSL. Birmensdorf.
- Burns, P., A. Nolin (2014) Using atmospherically-corrected Landsat imagery to measure glacier area change in the Cordillera Blanca, Peru from 1987 to 2010, *Remote Sensing of Environment* 140:165–178
- Carey, M. (2010) In the Shadow of Melting Glaciers: Climate Change and Andean Society, Oxford Univ. Press, New York.
- Carey, M., C. Huggel, J. Bury, C. Portocarrero, W. Haeberli (2012) An integrated socio-environmental framework for glacier hazard management and climate change adaptation: Lessons from Lake 513, Cordillera Blanca, Peru, *Climatic Change* 112:733–767.
- Chander, G. and B. Markham (2003) Revised Landsat-5 Tm Radiometric Calibration Procedures and Post Calibration Dynamic Ranges. *IEEE Transactions on Geoscience and Remote Sensing* 41:2674–2677.
- Chander, G., B.L. Markham, D.L. Helder (2009) Summary of Current Radiometric Calibration Coefficients for Landsat MSS, TM, ETM+, and EO-1 ALI Sensors. *Remote Sensing of Environment* 113:893–903.
- Chow, V. T. (1959) Open Channel Hydraulics. Caldwell, New Jersey, USA: The Blackburn Press.
- Christen, M., P. Bartelt, U. Gruber (2005) Numerical calculation of snow avalanche runout distances. In: Soibelman, L.; Pena-Mora, F. (eds) *Computing in Civil Engineering. Proc. of the 2005 International Conference*, July 12-15, 2005. Cancun, Mexico. 11 p.
- Christen, M., P. Bartelt, J. Kowalski, L. Stoffel (2008) Calculation of dense snow avalanches in three-dimensional terrain with the numerical simulation program RAMMS. In: *International Snow Science Workshop 2008, Proceedings*. September 21-27. Whistler, BC, CAN. 709-716.
- Christen, M., J. Kowalski, P. Bartelt (2010) RAMMS: numerical simulation of dense snow avalanches in three-dimensional terrain. *Cold Regions Science and Technology* 63, 1–14.

- DHI - Danish Hydraulics Institute (2001) MIKE 11 Reference manual, Appendix A. Scientific background.
- Diario La Republica (2010-04-20). Retrieved 04 24, 2010, www.larepublica.pe/regionales/20/04/2010/declaran-en-emergencia-la-laguna-palcacocha-en-huaraz.
- Emmer, A. and V. Vilímek (2013) Review Article: Lake and breach hazard assessment for moraine-dammed lakes: an example from the Cordillera Blanca (Peru), *Nat. Hazards Earth Syst. Sci.*, 13, 1551–1565.
- Emmer, A. and V. Vilímek (2014) New method for assessing the potential hazardousness of glacial lakes in the Cordillera Blanca, Peru, *Hydrol. Earth Syst. Sci. Discuss.*, 11, 2391–2439
- Evans, S.G. and J.J. Clague (1988) Catastrophic rock avalanches in glacial environments. *Proc. Fifth Int. Symp. on Landslides*, Vol. 2, pp. 1153-1158.
- Fiebiger, G. (1997) Hazard Mapping in Austria. *Journal of Torrent, Avalanche, Landslide and Rockfall Engineering* 134, Vol.61.
- Fischer, L., R. S. Purves, C. Huggel, J. Noetzli, and W. Haeberli (2012) On the influence of topographic, geological and cryospheric factors on rock avalanches and rockfalls in high-mountain areas. *Nat. Hazards Earth Syst. Sci.*, 12, 241–254.
- Flo-2D (2009) Flo-2D User’s Manual, FLO-2D Software, Inc., Nutrioso, AZ
- Flow Science (2012) FLOW-3D Documentation: Release 10.1.0, Flow Science, Inc.
- Forzieri, G., M. Degetto, M. Righetti, F. Castelli, and F. Preti (2011) Satellite Multispectral Data for Improved Floodplain Roughness Modelling. *J. Hydrology* 407:41–57.
- Forzieri, G., G. Moser, E.R. Vivoni, F. Castelli, and F. Canovaro (2010) Riparian Vegetation Mapping for Hydraulic Roughness Estimation Using Very High Resolution Remote Sensing Data Fusion. *J. Hydraulic Engineering* 136:855–867.
- Fread, D. L. (1979) DAMBRK: The NWS dam-break flood forecasting model. National Weather Service, Office of Hydrology, Silver Spring, MD.

- Froehlich, D. C. (1995) Peak outflow from breached embankment dam. *J. Water Resources Planning and Management*, 121(1), 90-97.
- Frey, H., W. Haerberli, A. Linsbauer, C. Huggel, and F. Paul (2010) A multi-level strategy for anticipating future glacial lake formation and associated hazard potentials. *Nat. Hazards Earth Syst. Sci.*, 10, 339–352.
- Garcia, R, J.L. López, M.E. Noya, *et al.* (2003) Hazard mapping for debris flow events in the alluvial fans of northern Venezuela. Third International Conference on Debris-Flow Hazards Mitigation: Mechanics, Prediction and Assessment. Davos, Switzerland.
- García, R., J.L. López, M.E. Noya, M.E. Bello, N. González, G. Paredes, and M.I. Vivas (2002) Hazard maps for debris and debris flow events in Vargas State and Caracas. Avila Project Report. Caracas, Venezuela, (In Spanish).
- Haerberli, W. (2013) Mountain permafrost — research frontiers and a special long-term challenge. *Cold Regions Science and Technology* 96: 71–76.
- Haerberli, W., J. Noetzli, L. Arenson, R. Delaloye, I. Gärtner-Roer, S. Gruber, K. Isaksen, C. Kneisel, M. Krautblatter, M. Phillips (2010) Mountain permafrost: development and challenges of a young research field. *Journal of Glaciology* 56 (200), 1043–1058 (special issue).
- Hamandawana, H., F. Eckardt, and S. Ringrose (2006) The Use of Step-wise Density Slicing in Classifying High-resolution Panchromatic Photographs. *International Journal of Remote Sensing* 27:4923–4942.
- Hegglin, E., and C. Huggel (2008) An integrated assessment of vulnerability to glacial hazards. *Mountain Research and Development* , 28, 299-309.
- Heller, V., W. H. Hager, and H. E. Minor (2009) Landslide generated impulse waves in reservoirs—Basics and computation. *VAW-Mitteilung*, Vol. 211, R. Boes, ed., ETH Zurich, Zurich.
- Horizons - Horizons South America S.A.C. (2013) Informe Técnico del Proyecto, Consultoría Para El Levantamiento Fotogramétrico Detallado De La Sub Cuenca Del Río Quillcay Y La Ciudad De Huaraz Para El Proyecto, Implementación de Medidas de Adaptación al

Cambio Climático y Gestión de Riesgos en la Sub-cuenca Quillcay (IMACC-QUILLCAY) - BID-MINAM (PE-T 1168), Ministerio Del Ambiente A Travel Del Fonam – Administrador De Los Recursos Del BID, Lima, Peru.

Hossain, A.K.M.A., Y. Jia, and X. Chao (2009) Estimation of Manning's Roughness Coefficient Distribution for Hydrodynamic Model Using Remotely Sensed Land Cover Features. 2009 17th International Conference on Geoinformatics. IEEE, pp. 1–4.

Huggel, C., N. Salzmann, S. Allen, J. Caplan-Auerbach, L. Fischer, W. Haeberli, C. Larsen, D. Schneider, R. Wessels (2010) Recent and future warm extreme events and high-mountain slope stability. *Philosophical Transactions of the Royal Society A: Mathematical, Physical, and Engineering Sciences* 368, 2435–2459.

Instituto Nacional de Defensa Civil. (2011) Informe de peligro N° 003-12/05/2011/COEN-SINADECI/ 15:00 horas (Informe N° 01): Peligro por aluvión en el departamento de Ancash. Huaraz-Peru: COEN-SINADECI.

IPCC - Intergovernmental Panel on Climate Change (2013) *Climate Change 2013: The Physical Science Basis. Working Group I Contribution to the IPCC 5th Assessment Report - Working Group I contribution to the IPCC 5th Assessment.* IPCC, Geneva, Switzerland.

Julien, P. Y. (2010) Erosion and Sedimentation, second edition (p. 371). Cambridge, UK: Cambridge University Press.

Julien, P. Y. and C. A. Leon (2000) Debrisfloods and Debris Flows Classification, Rheology and Structural Design. In Invited paper at the International Workshop on Mudflows and debris flows, Caracas, Venezuela, November 27- December 1.

Kattleman, R. (2003) Glacial Lake Outburst Floods in the Nepal Himalaya: A Manageable Hazard? *Natural Hazards* 28: 145–154.

Laenen, A., K. M. Scott, J. E. Costa, L. L. Orzol (1987) Hydrologic hazards along Squaw Creek from a hypothetical failure of the glacial moraine impounding Carver Lake near Sisters, Oregon. U.S. Geological Survey, Open-File Report 87-41.

National Institute of Civil Defense of Peru (2011) Report of Hazard 003-12/05/2011. Lima.

- MacDonald, T. C. and J. Langridge-Monopolis (1984) Breaching characteristics of dam failures. *Journal of Hydraulic Engineering*, 110(5), 567-586.
- O'Brien, J.S. (2003) FLO-2D User's Manual (Version 2003.06), FLO-2D, Nutrioso, AZ
- O'Connor, J. E., J. H. Hardison III, J. E. Costa (2001) Debris Flows from Failures of Neoglacial-Age Moraine Dams in the Three Sisters and Mount Jefferson Wilderness Areas, Oregon. U.S. Geological Survey professional paper, (1606).
- OFEE, OFAT, ODEFP (Switzerland) Ed. (1997) *Prise en compte des dangers dus aux crues dans le cadre des activités de l'aménagement du territoire*, (OFEE), (OFAT), (OFEFP), Bienne.
- Peng, M., L. M. Zhang (2012) Breaching parameters of landslide dams. *Landslides* 9:13–31.
- Portocarrero, C. (2014) *The Glacial Lake Handbook: Reducing Risk from Dangerous Glacial Lakes in the Cordillera Blanca, Peru*, United States Agency for International Development, Washington, DC.
- Raetzo, H. Raetzo, O. Lateltin, D. Bollinger, J. Tripet (2002) Hazard assessment in Switzerland – Codes of Practice for mass movements, *Bulletin of Engineering Geology and the Environment*, 61(3), 263–268.
- Richardson, S. D. and J.M. Reynolds (2000) An overview of glacial hazards in the Himalayas. *Quaternary International*, 65/66, 31–47.
- Rickenmann, D. (1999) Empirical Relationships for Debris Flows. *Natural Hazards*, 19, 47–77.
- Rivas, D., D. McKinney, B. Hodges (2014) Predicting outflow induced by dam moraine failure in glacial lakes: the Lake Palcacocha case from an uncertainty perspective. *J. of Hydrology* (in review).
- Rosenzweig C, G Casassa, DJ Karoly, A Imeson, C Liu, A Menzel, S Rawlins, TL Root, B Seguin, P Tryjanowski (2007) Assessment of observed changes and responses in natural and managed systems. In: Parry ML, Canziani OF, Palutikof JP, van der Linden PJ, Hanson CE (eds) *Climate Change 2007: Impacts, Adaptation and Vulnerability. Contribution of Working Group II to the Fourth Assessment Report of the Intergovernmental Panel on Climate Change*. Cambridge University Press, Cambridge, pp 79–131.

- Rouse, J.W., D.W. Deering, and J.A. Schell (1973) Monitoring the Vernal Advancement and Retrogradation (green Wave Effect) on Natural Vegetation. Prog. Rep. RSC 1978-1, Remote Sensing Center, Texas A&M Univ., College Station, 93p. (NTIS No. E73-106393.
- Schneider, D., C. Huggel, A. Cochachin, S. Guillén, J. García (2014) Mapping hazards from glacial lake outburst floods based on modelling of process cascades at Lake 513, Carhuaz, Peru. *Adv. Geosci.*, 35, 145–155, 2014.
- UGRH – Unidad de Glaciología y Recursos Hidricos (2009) Autoridad Nacional de Agua (ANA) de Peru.
- UGRH – Unidad de Glaciología y Recursos Hidricos (2010) Area de Inventario de Glaciares y Lagunas, Autoridad nacional del Agua, Direccion de Conservacion y Planeamiento de Recursos Hidricos, Huaraz.
- Walder, J. S., J. E. O'Connor (1997) Methods for predicting peak discharge of floods caused by failure of natural and constructed earthen dams. *Water Resour. Res.* 33(10): 2337-2348.
- WGMS – World Glacier Monitoring Service (2012) Fluctuations of Glaciers 2005-2010 (Vol. X). Zemp, M., Frey, H., Gärtner-Roer, I., Nussbaumer, S.U., Hoelzle, M., Paul, F. and W. Haeberli (eds.), ICSU (WDS) / IUGG (IACS) / UNEP / UNESCO / WMO, World Glacier Monitoring Service, Zurich, Switzerland: 336 pp. Publication based on database version: doi:10.5904/wgms-fog-2012-11.
- Xu, Y., L. M. Zhang (2009) Breaching Parameters for Earth and Rockfill Dams *J. Geotech. Geoenviron. Eng.* 2009.135:1957-1970.